# Trabalho de Conclusão de Curso

## Thermal relic Dark Matter: a review of production mechanisms

Gabriela Alevi Dagrela[1]

[1] *Centro de Ciências Naturais e Humanas, Universidade Federal do ABC, Santo André-SP, Brasil*

In this work, four mechanisms known in the literature for Dark Matter creation in the early universe were analysed. The mechanisms were studied assuming simplified interactions between the dark sector and the Standard Model. Numerical results were obtained using the framework of Boltzmann equations for the relevant particle species. In addition, the dependence of the Dark Matter relic abundance on the model parameters was investigated.

### 1. INTRODUCTION

The existence of Dark Matter (DM) has been hinted and corroborated by numerous experimental data in the last century. Current estimates indicate that Dark Matter compounds 26,5% of our Universe [1], which leads to questions about its formation and structure.

The first proof for Dark Matter presence emerged in 1932, with Jan Oort. When studying the quantity and velocity of stars in the Milky Way, Oort noticed that the mass of visible stars was too small to account for all the gravitating matter that was supposed to exist in this region, implied by the velocities of the bodies near [2]. By analysing the Doppler shift the light emitted by these stars suffered, he was able to calculate each star velocity, reaching the conclusion that these stars were moving fast enough to escape the gravitational resistance of the galaxy. However, these stars remained in their orbit, which could not be explained at the time. Oort considered possible the existence of errors in the measurements of the stars' masses, therefore providing a solution in accord with the understanding of his time. He did not consider the existence of non-baryonic matter.

Then, Fritz Zwicky (1933) independently noted that the velocities of stars found in the Coma cluster required a mass density at least 400 times bigger than what was calculated from visible matter to keep them in orbit [3]. By employing the Doppler shift technique to calculate the velocities of the stars in the Coma cluster, he was able to find their kinetic energy, and hence, by considering that the stars only interacted through Newtonian gravity, he obtained their potential

energy through the Virial Theorem:

$$\langle K \rangle = -\frac{1}{2}\langle U \rangle \tag{1}$$

Using Newton's Gravitational Law, he calculated the total mass for the cluster. However, Zwicky overestimated the mass-to-light ratio (the total mass of the cluster divided by its luminosity) of this cluster, by using a wrong value for the Hubble rate $H_0$. In reality, the Coma cluster mass would have to be 50 times bigger than the mass-to-light ratio evaluated to maintain its stars in orbit. [4]. Three years later, Smith (1936) discovered that the same pattern could be found in the Virgo cluster [5], where the mass calculated through the Virial Theorem was $1000 M_\odot$ ($M_\odot$ is the mass of the Sun) larger than what was visible in the cluster.

Following this discovery, Babcock (1939), by analysing the spectra of the Andromeda galaxy, found that the outer regions of the galaxy were rotating with a higher velocity than the center, which could be explained by a higher mass-to-light ratio in the outskirts, or strong light absorption by dust in the center [6].

Later, in the 1970s, Vera Rubin and her collaborators, after analysing the rotation curves of 67 emission nebulae (areas filled of hydrogen, whose atoms get excited by the radiation emitted by young stars in the vicinity) in the Andromeda galaxy, found the same result. According to the classical prediction:

$$v(r) = \sqrt{\frac{Gm(r)}{r}}, \tag{2}$$

where $m(r)$ is the mass enclosed inside radius $r$. The results found in Rubin's work implies that, as $r$ grows, $m(r)$ must increase as well [7].

Also in the 1970s, the gravitational lensing technique was discovered. This method is derived from Einstein's General Relativity, and consists of observing the path of a light ray passing close to a massive object. The mass will bend the space-time fabric, altering the path of light. This mechanism not only allows for the measurement of a galaxy total mass, but also how this mass is distributed throughout the space [8]. Bergmann, Petrosian and Lynds (1990) found that, for the Abell 370 cluster, the mass-luminosity ratio should be bigger by a factor of $10^2$ - $10^3$ $M_\odot/L_\odot$ to account for all the mass encountered through lensing [9]. The same pattern was found in other clusters and galaxies, in the last years [10].

Important evidence also came from the merging of the Bullet galaxy cluster (1E 0657-56). Two different galaxy clusters approached each other and collided. The majority of their baryonic matter

exists as super hot gas inside both bodies, that was heated up by the collision and emitted a huge amount of X rays, which were observed by the Chandra Observatory. The gas was slowed down due to fluid resistance, reducing its initial velocity. However, comparing these observations with gravitational lensing shows that the majority of the clusters' mass is not in the gas region, but following the predicted paths for both bodies, if the collision had not occurred, with the same initial velocity. Therefore, it is necessary that more mass is 'hidden' to account for the gravitational pull observed, and that this mass does not interact with baryonic matter [11]. The same pattern was observed by Bradač et al (2008) in the merging cluster MACS J0025.4-1222 [12].

While cosmological techniques have enabled many discoveries about Dark Matter properties, such as its current low temperatures [13], and its distribution on our Universe, its non-gravitational properties remain a mystery, such as its mass and the interactions it participates in. Different theoretical models were proposed to explain how particle Dark Matter interacts, both with the Standard Model and with possible additional particles in the dark sector, as well how these reactions would affect the formation of cosmological structure [14–16].

In this work, we discuss some of the most popular mechanisms found in literature for production of the observed Dark Matter relic density, focusing specifically in Dark Matter as a thermal relic. To achieve this objective, we derive the relevant Boltzmann equations, which allows us to calculate the Dark Matter population as a function of temperature. In Sec. 2 we briefly review the Standard Model and the Standard Cosmological Model, and the necessary formalism for developing the Boltzmann equations in Sec.3. Sec.4 is dedicated to the discussion of four production mechanisms: freeze-out, co-annihilation, conversion driven freeze-out and freeze-in. Finally, in Sec.5, we present our conclusions. Appendix A contains a detailed derivation of the Boltzmann equations presented in Sec. 3.

## 2. FUNDAMENTAL CONCEPTS

### 2.1. Standard Model

Despite all the proof about Dark Matter existence mentioned previously, particle Dark Matter properties remain unknown, as well as how it could interact with the already known particles. The discovered particles that exist in our Universe compound what is called the Standard Model.

The Standard Model (SM) is a framework that aims to describe all the existing particle species in the Universe, and how they interact with each other. It explains successfully the experimental

data observed in colliders and observatories, and allows for a better understanding of the forces that run our Universe. The model considers 3 fundamental forces, that cause particles to interact: the electromagnetic force, the weak nuclear force, and the strong nuclear force. Note that despite its huge success, the SM does not include the gravitational force. It also considers the existence of several fundamental particles, that can not be subdivided into smaller pieces. These can be separated in two groups: the fermions and the bosons.

The fermions are particles with a half-integer spin, and are responsible for building matter. They can also be subdivided in two groups: the quarks and the leptons. There are 6 quarks, that compose 3 generations: the up and the down (first generation), the charm and the strange (second generation), the top and the bottom (third generation). The generations have very different mass ranges, with the first generation being the least massive. Due to this, the first generation is the only stable one (it does not decay in other particles), and is responsible for forming all the ordinary matter on Earth. The second and third generations decay rapidly, and can only be found in high energy environments. The quarks are always found in the form of hadrons, consisting of two quarks (mesons) or three quarks (baryons), held together by the strong nuclear force. The baryons are responsible for forming the majority of the known matter, thus the ordinary matter is called Baryonic Matter. The two most important baryons are the proton and the neutron. Besides the strong nuclear force, the quarks also interact through the weak force and the electromagnetic force. Each quark also has its own anti-quark, which has the same mass but opposite charge of the original quark. When a particle and a antiparticle react, they annihilate each other, and release energy.

There are 3 charged leptons: the electron, the muon and the tau. As occurs with the quarks, only the first generation lepton (electron) is stable due to its smaller mass, and is responsible for forming atoms. The muon and the tau both decay rapidly, and are only seen in high energy backgrounds. The leptons interact through the weak nuclear force (responsible for particle decay) and the electromagnetic force. Each charged lepton also has a corresponding neutrino: the electron neutrino, the muon neutrino and the tau neutrino. The neutrinos are very light particles with neutral charge, that only interact through the weak nuclear force. Hence, the neutrinos are very hard to be detected.

The other group of the Standard Model are the bosons, particles with a integer spin. Bosons are force carriers, responsible for transmitting the three fundamental forces, and mediating the interaction between the fermions. The photon is the boson related to the electromagnetic force, while the $W^{\pm}, Z^{0}$ are responsible for the weak force and the gluons mediate the strong force.

Finally, the Higgs boson is responsible for generating mas to the weak bosons and the fermions (with the exception of neutrinos).

Despite all its structure, the Standard Model is not complete, and does not account for the existence of Dark Matter. Hence, the experimental observations that point to the presence of DM also hints to the fact that the Standard Model needs to be expanded.

### 2.2. Standard Cosmological Model

Another important model used to describe our Universe is the $\Lambda CDM$ model, also known as the Standard Cosmological Model, that details how our Universe behaves, along with its history. It considers the Universe to be comprised of four main components: radiation, baryonic matter, cold dark matter (CDM), and a cosmological constant $\Lambda$, which will be explained later. This framework considers that, at large scales, the Universe is homogeneous, isotropic and flat, with the large extensions of vacuum compensating for the matter clumps, which known as the Cosmological Principle (CP). Lastly, it assumes that Einstein's General Relativity Theory correctly describes the way gravitational interactions occur, and that the Big Bang theory correctly delineate how our Universe began [17]. We shall analyse the main features of this model.

The Big Bang theory conveys a Universe with a changing size. The first evidence that our Universe is expanding came from the observations of Edwin Hubble. Stars and nebulae emit light in specific wavelengths, determined by their chemical composition. Those are the emission lines, caused by electron excitation. Hubble noticed that the light coming from distant bodies presented a shift in its emission lines, making the stripes closer to the red side of the visible spectrum [18]. This phenomenon was nominated *redshift*, usually quantified by the parameter $z$:

$$1 + z = \frac{\lambda_{observed}}{\lambda_{emitted}} \tag{3}$$

Hubble's biggest achievement was noticing that the redshift in the observed spectrum means that the light emitter is moving away from Earth, which would be expected in an expanding Universe. He also realized that the velocity with which the object is moving away is proportional to the distance $d$ between the object and Earth:

$$v = H_0 d, \tag{4}$$

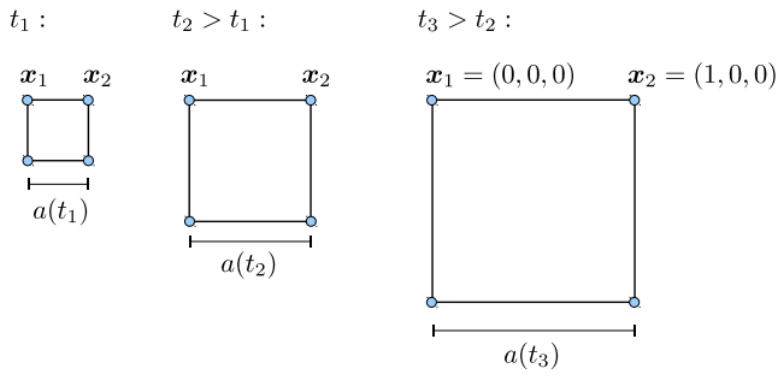


FIG. 1: A visual representation of how the distance of two objects change with Universe expansion. The comoving distance between points $x_1$ and $x_2$ remains 1, but the grid size increases with time [19].

where $H_0$ represents the Hubble rate, and the 0 subscript indicates its current value. Hence, further away galaxies have higher velocities.

In order to understand the above relation it is useful to introduce the scale factor $a$, which increases with time. It is used to express how the distance $d$ between two objects change as times passes:

$$d(t) = a(t)d(t = 0) \tag{5}$$

By convention, we set $a = 1$ today. The way the scale factor behaves with time is determined by the Friedmann Equation, derived from Einstein's General Relativity by Alexander Friedmann [20] (which is in accordance with the $\Lambda CDM$ assumptions of isotropy and homogeneity):

$$H^2 = \left(\frac{\dot{a}}{a}\right)^2 = \frac{8\pi G}{3}\rho(t) - \frac{\kappa}{R_0^2 a^2}, \tag{6}$$

where $\rho(t)$ represents the total energy density of the Universe and $G$ is the Newtonian Constant of Gravitation. For this equation, and for the following analysis, we adopt the usage of natural units ($c = \hbar = 1$). The second term relates to the geometry of our Universe: $\kappa > 0$ represents an elliptical geometry, $\kappa = 0$ an Euclidean geometry, and $\kappa < 0$ an hyperbolic geometry. Finally, $R_0$ is the curvature radius for the Universe. According to recent estimates, cosmological evidence points that our Universe is very close to flat [1], as considered in the $\Lambda CDM$ model. Hence, from now on, we take $\kappa = 0$.

Using Eq. 6 and computing the second derivative of the scale factor:

$$\dot{a} = Ha \Rightarrow \ddot{a} = \dot{a}H + a\frac{dH}{dt} \tag{7}$$

But:

$$\begin{aligned} H &= \sqrt{\frac{8\pi G}{3}\rho(t)} \Rightarrow \frac{dH}{dt} = \frac{1}{2}H\frac{\dot{\rho}}{\rho} \\ &\Rightarrow \ddot{a} = \dot{a}H + a\frac{H}{2}\frac{\dot{\rho}}{\rho} \\ &\Rightarrow \ddot{a} = \frac{\dot{a}^2}{a} + \frac{\dot{a}}{2}\frac{\dot{\rho}}{\rho}, \end{aligned} \tag{8}$$

where we have used $\dot{a} = Ha$ in the last step. Therefore, in order to determine $a(t)$ we must also determine how the energy density evolves with time.

The time evolution of $\rho$ can be determined under some simplifying assumptions. We begin by considering the First Law of Thermodynamics:

$$dQ = dU + dW \tag{9}$$

where $dQ$ is the heat that enters or exits a specific region in space, $dU$ is the energy variation in this determined region, and $dW$ is the work made inside this area. If we consider this volume to be expanding, we can write:

$$dW = PdV \Rightarrow dQ = dU + PdV, \tag{10}$$

where $P$ is the system's external pressure, and $dV$ represents the change in volume.

If our Universe is homogeneous, then there is no relevant flow of heat into any region in space. Therefore $dQ = 0$, and the expansion is an adiabatic process. Consequently, the expansion does not increase entropy, which would be expected if we assume that the total entropy in our Universe is constant (entropy density, however, still changes due to the expansion).

Therefore:

$$dU + PdV = 0 \tag{11}$$

If we choose our system to be a sphere of radius $R(0) = 1$, that changes with time as $R(t) = R(0)a(t) = a(t)$, its volume will be:

$$V = \frac{4}{3}\pi a(t)^3 \Rightarrow dV = 4\pi a(t)^2\frac{da(t)}{dt} \tag{12}$$

Choosing the energy density of this area to be $\rho$, the total internal energy $U$ inside this sphere is:

$$U = \frac{4}{3}\pi a(t)^3\rho \Rightarrow dU = 4\pi a(t)^2\frac{da(t)}{dt}\rho + \frac{4}{3}\pi a(t)^3\frac{d\rho}{dt} \tag{13}$$

Finally, substituting Eqs.12 and 13 in Eq.11:

$$\begin{aligned} 4\pi a(t)^2\dot{a}(P+\rho) + \frac{4}{3}\pi a(t)^3\dot{\rho} = 0 \\ \Rightarrow \dot{\rho} + 3\frac{\dot{a}}{a}(P+\rho) = 0 \end{aligned} \tag{14}$$

This is the Fluid Equation, and it defines how the Universe's energy density and pressure changes with time. Combining Fluid Equation with Friedmann Equation, we obtain:

$$\frac{\ddot{a}}{a} = \frac{-4\pi G}{3}(\rho + 3P) \tag{15}$$

which determines how the Universe acceleration evolves with time.

From this equation, it is possible to see that, if both energy density ($\rho$) and pressure ($P$) are positive, then Universe expansion should be slowing down. However, from observations of galaxy velocities, we know this is not true. The expansion rate is actually increasing with time. This is hinted by observations of Type Ia Supernovae, as shown by Riess et al. (1998) [21] and Perlmutter et al (1997) [22]. By analysing the redshift and the brightness of distant Type Ia Supernovae, they noted that, in the distant past (high redshift), the distance between the Earth and the Supernovae are larger than would be expected if the expansion rate $H$ was constant. Hence, the expansion must be accelerating.

Today, the main theory to explain this acceleration phenomenon is *Dark Energy* [23]. In the $\Lambda CDM$ model, Dark Energy is a cosmological constant $\Lambda$, related to an intrinsic vacuum energy [24]. Analysis of anisotropies present in the Cosmic Microwave Background (CMB) predict that almost 68% of our Universe is made of Dark Energy [25].

The $\Lambda CDM$ model considers that our Universe is made of 31% of matter (both baryonic and dark), 68% of Dark Energy (as mentioned previously), and the rest of radiation. However, this scenario was not always true. Right after the Big Bang, the Universe was dominated by radiation.

In order to understand how the densities of each component and scale factor evolved during these times, we must first determine how the pressure is related to the energy density. For a non-relativistic and ideal gas we can use the perfect gas law:

$$PV = NkT \Rightarrow P = \frac{N}{V}kT \tag{16}$$

where $k$ is Boltzmann's constant, $T$ the gas temperature and $N/V = n$ the particle density. But, from the kinetic theory:

$$3kT = m\langle v^2 \rangle \tag{17}$$

being $\langle v^2 \rangle$ the root mean square thermal velocity of the particles and $m$ their mass. Since for non-relativistic particles $v \ll 1$, we have $kT \simeq 0$ and therefore:

$$P \simeq 0 \text{ (non-relativistic gas)} \tag{18}$$

In the case of a gas of photons, its energy density is given by [26]:

$$\rho = n\langle E \rangle = np \text{ and } 3kT = p \tag{19}$$

where $p$ is the average 3-momentum of the particles. Therefore:

$$\begin{aligned} \rho &= 3(nkT) = 3P \\ \Rightarrow P &= \tfrac{1}{3}\rho \text{ (relativistic gas)} \end{aligned} \tag{20}$$

Lastly, for Dark Energy we assume [24]:

$$P = -\rho \text{ (Dark Energy)} \tag{21}$$

All the above gases can be parameterized as:

$$P = w\rho \tag{22}$$

where $w = 0, 1/3, -1$ for matter, radiation and Dark Energy, respectively.

Using the above results, we can finally integrate the Fluid Equation:

$$\rho(t) = \int \dot{\rho} dt = \int -3\frac{\dot{a}}{a}(P + \rho) dt \tag{23}$$

Then, using Eq. 22, we obtain:

$$\rho(t) = \int -3\frac{\dot{a}}{a}\rho(1 + w) dt \tag{24}$$

Therefore:

$$\int \frac{1}{\rho}\frac{d\rho}{dt} dt = \int \frac{-3(1 + w)}{a}\frac{da}{dt} dt \tag{25}$$

$$\log\left(\frac{\rho}{\rho_0}\right) = -3(1+w)\log\left(\frac{a}{a_0}\right) \tag{26}$$

Using logarithms properties:

$$\log\left(\frac{\rho}{\rho_0}\right) = \log\left(\frac{a}{a_0}\right)^{-3(1+w)} \tag{27}$$

$$\rightarrow \rho = \rho_0\left(\frac{a_0}{a}\right)^{3(1+w)} \tag{28}$$

Hence:

$$\begin{aligned} \rho_M &= \rho_{M,0}\left(\frac{a_0}{a}\right)^3 \text{ (matter)} \\ \rho_R &= \rho_{R,0}\left(\frac{a_0}{a}\right)^4 \text{ (radiation)} \\ \rho_{DE} &= \rho_{DE,0} \text{ (Dark Energy)} \end{aligned} \tag{29}$$

Through this, we can see that radiation density decreases faster than matter density, and that dark energy density is constant. The difference between the expressions for radiation and matter densities can be explained through redshift. As the Universe expands, the wavelength of radiation increases by a factor $a$. But the energy of a wave is given by:

$$E = \frac{2\pi}{\lambda} \tag{30}$$

where $\lambda$ is its wavelength. Therefore, as the wavelength increases by a factor $a$, the energy decreases by the same factor $a$. So, radiation energy density decreases by the variation of the total volume of the Universe, but also by the redshift it suffers in this process.

Today, the measured energy densities, for radiation, baryonic matter, Dark Matter, and Dark Energy are, respectively [1]:

$$\begin{aligned} \rho_R &\approx 4.64 \times 10^{-34}\text{GeV}^4 \\ \rho_{BM} &\approx 4.20 \times 10^{-31}\text{GeV}^4 \\ \rho_{DM} &\approx 2.25 \times 10^{-30}\text{GeV}^4 \\ \rho_{DE} &= 5.83 \times 10^{-30}\text{GeV}^4 \end{aligned} \tag{31}$$

Employing these values and knowing how each density changes with $a$, we are able to estimate the initial energy densities $\rho_0$, and analyse how $\rho_{TOTAL}$ changed with time. The result is that,

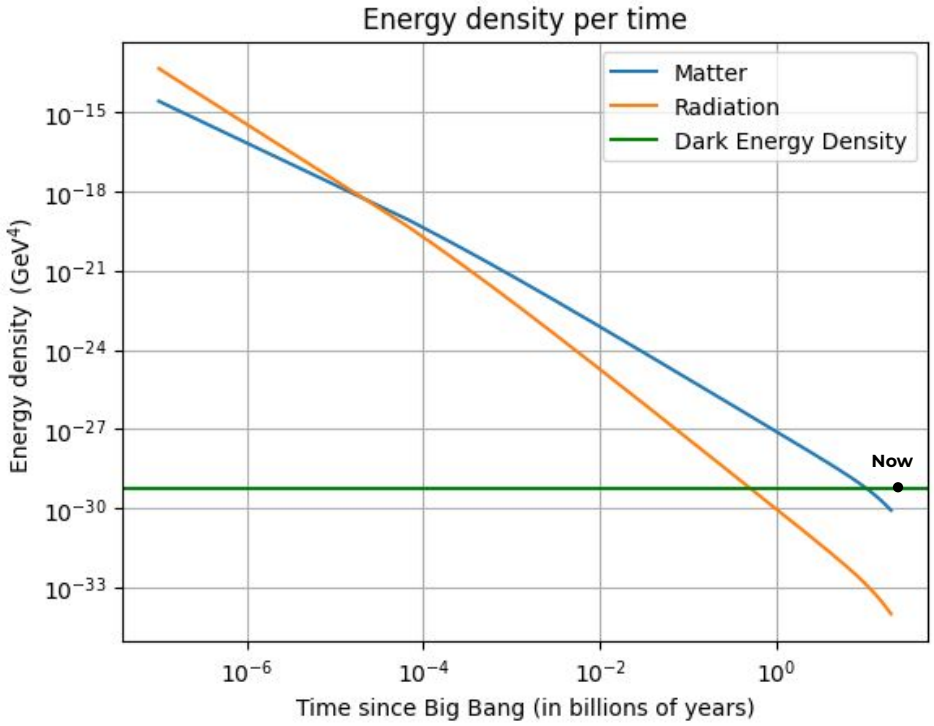


FIG. 2: Energy densities of radiation, matter and dark energy through time, since the Big Bang.

for the approximate first 50 thousand years after the Big Bang, the Universe was dominated by radiation [1]. Afterwards, we arrive at a point where matter and radiation had the same density, known as the matter-radiation equality. Following this moment, we enter an era where the dominant component of the Universe was matter. Lastly, when the Universe was approximately 8 billion years old, dark energy density became bigger than matter density. This evolution can be seen in Fig. 2.

Since, from Eq. 15 we have that the rate of expansion and its acceleration depend on the $\rho$ and $P$, as $\rho$ changes with time, the velocity of the expansion of our Universe changes as well. Therefore, the different Eras of the Universe have different expansion rates, and specific characteristics that come with it, as can be seen in Fig. 3.

According to the Big Bang theory, the Early Universe was much smaller and incredibly denser than nowadays, with extremely high temperatures. It was populated by Standard Model particles, along with particles that have not been discovered yet (among them, the DM particle). The energy density was considerably large, which lead Standard Model particles to have great velocities, hence being relativistic. This made it impossible for particles to form stable nuclei or atoms, meaning that all matter existed in a plasma of leptons, quarks and gluons. The reaction rate $\Gamma$ of these particles was much larger than the Hubble expansion rate $H$, allowing thermal equilibrium to be

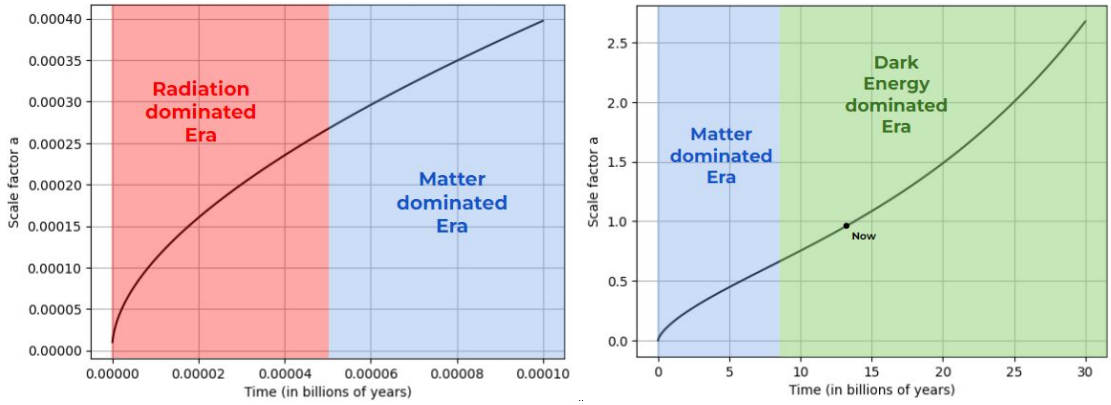


FIG. 3: Scale factor $a$ per time, since Big Bang

maintained in the thermal bath [27].

### 2.3. Equilibrium Thermodynamics

A particle species is said to be in thermal equilibrium when its reaction rate $\Gamma$ is bigger than the Hubble expansion rate $H$, implying that particles are able to react before they are separated due to Universe expansion. When the thermal bath is in equilibrium, its energy is uniformly distributed throughout all of its components, determining some of the species properties, such as number density $n$:

$$n = \frac{g}{(2\pi)^3} \int f(\vec{p}) d^3p \tag{32}$$

where $g$ is the number of internal degrees of freedom and $f(\vec{p})$ is the species phase space occupancy.

The internal degrees of freedom of a particle species is the number of variables that can be altered without breaking any constraints of the system. For an electron in a Hydrogen atom, the spin is an internal degree of freedom: both spin-up and spin-down cases are possible. The phase space is a space that contains all the possible states for the particles in the system in consideration. In this context, the phase space occupancy describes how many particles are in each possible state, labeled according to their momentum $\vec{p}$.

In a reaction $a + b \leftrightarrow c + d$, both directions of the reaction will exchange energy and momentum. When both directions exchange energy and momentum at the same rate, thus maintaining the total energy and momentum of all the interacting species constant (i.e. the total energy and the total momentum of $a, b, c, d$ are not altered due to the reaction), these particles are said to be in kinetic equilibrium.

For the case of a species in kinetic equilibrium, the phase space occupancy is given by:

$$f(\vec{p}) = [\exp((E+\mu)/T) \pm 1]^{-1} \tag{33}$$

where the + sign stands for Fermi-Dirac statistics and the − sign stands for Bose-Einstein statistics. The parameter $\mu$ represents the particle's chemical potential. It stands for the rate of change in the systems free energy when the species particle number is altered, while maintaining the pressure and the temperature constants. If we consider a reaction:

$$a + b \leftrightarrow c + d \tag{34}$$

the particles' chemical potential will define which direction of the reaction will prevail. If $\mu_a + \mu_b > \mu_c + \mu_d$, reaction $a + b \rightarrow c + d$ will occur more frequently than its opposite direction. If $\mu_a + \mu_b < \mu_c + \mu_d$, reaction $c + d \rightarrow a + b$ will take place more often than the other possible direction. If $\mu_a + \mu_b = \mu_c + \mu_d$, the system is said to be in chemical equilibrium, and both directions will balance each other, keeping the populations of $a, b, c, d$ constant. For the following calculations, we assume chemical equilibrium, and therefore neglect the effect of $\mu$.

Using Eq. 33 in Eq. 32:

$$\begin{aligned} n &= \frac{g}{(2\pi)^3} \int \frac{1}{\exp(E/T) \pm 1} d^3p \\ &= \frac{g}{(2\pi)^3} \int \frac{4\pi p^2}{\exp(E/T) \pm 1} dp \end{aligned} \tag{35}$$

For a relativistic species ($m \ll \vec{p}$), $E \simeq p$, and the phase space occupancy is given by:

$$f(p) = [\exp(p/T) \pm 1]^{-1} \tag{36}$$

Therefore, Eq. 35 for a particle $i$ becomes:

$$n = \frac{g}{(2\pi)^3} \int_0^\infty \frac{4\pi|p|^2}{\exp(p/T) \pm 1} dp \begin{cases} \frac{3}{4}\frac{\zeta(3) g_i T^3}{\pi^2} & \text{fermions} \\ \frac{\zeta(3) g_i T^3}{\pi^2} & \text{bosons} \end{cases} \tag{37}$$

where $\zeta$ is the Zeta Riemann function.

For any $\vec{p}$ value, our phase space occupancy is given by:

$$f(\vec{p}) = [\exp(E/T) \pm 1]^{-1} = [\exp((\sqrt{p^2 + m^2})/T) \pm 1]^{-1} \tag{38}$$

It is useful to rewrite Eq. 35 with a variable transformation $p = \sqrt{E^2 - m^2}$:

$$n = \frac{g}{2\pi^2} \int_m^\infty \frac{\sqrt{(E^2 - m^2)}}{\exp(E/T) \pm 1} E dE \tag{39}$$

In a semi-relativistic regime ($m \simeq \vec{p}$), $\exp(E/T)$ is much bigger than 1, so we can neglect the $\pm 1$ term, and approach that, at this regime, the number density at equilibrium is the same for fermions and bosons. Then, we define $x = E/m$, $dx = dE/m$:

$$\begin{aligned} n &= \frac{g}{2\pi^2}\int_1^\infty \frac{\sqrt{(x^2-1)}}{\exp(\frac{xm}{T})} x m^3 dx \\ &= \frac{g}{2\pi^2}\int_1^\infty m^3 \frac{d}{dz}\left(\frac{\sqrt{x^2-1}}{\exp(xz)}\right) dx \end{aligned} \tag{40}$$

where $z = m/T$. In this form, we can write:

$$\int_1^\infty \left(\frac{\sqrt{x^2-1}}{\exp(xz)}\right) = \frac{K_1(z)}{x} \tag{41}$$

where $K_1$ is the modified Bessel function of second kind, in the first degree.

$$n = \frac{g}{2\pi^2} m^3 \frac{d}{dz}\frac{K_1(z)}{z} = \frac{g}{2\pi^2} T m^2 K_2\left(\frac{m}{T}\right) \tag{42}$$

where $K_2$ is the modified Bessel function of second kind, in the second degree.

This result is valid for any case when $\exp(E/T)$ is much bigger than 1.

In a non-relativistic regime ($m \gg T$), the condition $\exp(E/T) \gg 1$ is still valid. In this case, using a series expansion at $m \to \infty$:

$$K_2(m/T) \to \exp(-m/T)\sqrt{\frac{\pi T}{2m}} \tag{43}$$

Hence, for a particle $i$ in equilibrium, in a non-relativistic regime:

$$\overline{n}_i = g_i \left(\frac{m_i T}{2\pi}\right)^{3/2} \exp(-m_i/T) \tag{44}$$

An important concept to analyse in the Early Universe is entropy. Entropy is the quantity that measures how disorganised is the system, or, how much of its energy is inaccessible to be turned into work. According to the Second Law of Thermodynamics, the entropy variation caused in a system by a spontaneous process (i.e. where there is no external influence in the system) must always be positive $\Delta S \geqslant 0$. Hence, if we model our Universe as a system, its entropy must always increase or remain constant (once there are no external agents acting on the system).

When a process increases the entropy in the system, it is increasing the fraction of the system's energy that can not be turned into work. Thus, this process is irreversible, once it is not possible to revert this energy into an accessible state. A process that maintains the entropy constant is a reversible process, once it is possible to undo the transformation without breaking any constraint.

All the reactions taking place in the plasma are reversible reactions, therefore they do not change the entropy of the system, and the entropy in the plasma is conserved.

In the Radiation Epoch, when the Dark Matter candidates we will analyse were created, entropy density is given by:

$$s = \frac{2\pi^2}{45} g_{*s}(T) T^3 \tag{45}$$

where $g_{*s}$ are the relativistic degrees of freedom associated with entropy:

$$g_{*s} = \sum_{\text{bosons}} g_i \left(\frac{T_i}{T}\right)^3 + \frac{7}{8} \sum_{\text{fermions}} g_i \left(\frac{T_i}{T}\right)^3 \tag{46}$$

where $T$ is the temperature of the plasma. Our Universe, as a system, has an entropy value proportional to its temperature. This total value of entropy is formed by contributions from each particle species' entropy, which depends on the particle's internal degrees of freedom. The relativistic degrees of freedom associated with entropy $g_{*s}$ represent a sum over all the internal degrees of freedom of each relativistic species (i.e. a sum over all the variables that do not affect entropy and that can be altered in each relativistic particle species without breaking any of the system's constraints). Each particle species' total entropy is proportional to the number of their internal degrees of freedom, thus, the total entropy in the Early Universe (when the majority of the Universe contents where relativistic particles) is proportional to $g_{*s}$. We can approach $g_{*s}$ as [28]:

$$\begin{aligned} g_{*s} &= 100,\ T \gtrsim 200\text{MeV} \\ g_{*s} &= 10,\ 200\text{MeV} > T \gtrsim 0.1\text{MeV} \\ g_{*s} &= 3,\ 0.1\text{MeV} > T \end{aligned} \tag{47}$$

During the Radiation Era, the Universe was dominated by radiation, which allows us to write [19, 24]:

$$\begin{aligned} \rho_{total} \simeq \rho_{radiation} \ &\Rightarrow\ \rho_{total} = \frac{\pi^2}{30} g_*(T) T^4 \\ &\Rightarrow\ T(t) = \left(\frac{45}{32\pi^2}\right)^{1/4} \frac{T_P}{\sqrt{t_P}} \frac{\sqrt{2H_0}}{a(t)} \end{aligned} \tag{48}$$

where $T_P = 1.41 \times 10^{32}$ K is the Planck temperature, $t_P = 5.39 \times 10^{-44}$ s is the Planck time, $H_0 = 67.4$ km/s Mpc is the Hubble rate value today, and $g_*$ is the effective number of relativistic degrees of freedom, which depends on the temperature. As mentioned previously, in a thermodynamic system, the number of degrees of freedom is the number of variables that can be modified in

a system, without breaking any constraints. For our Universe, we have an effective number of degrees of freedom, which sums over the internal degrees of freedom of all the existing particle species, to analyse how many variables inside our Universe can be modified without breaking any laws. The effective number of relativistic degrees of freedom takes this sum over the internal degrees of freedom of relativistic species, solely:

$$g_* = \sum_{\text{bosons}} g_i \left(\frac{T_i}{T}\right)^4 + \frac{7}{8} \sum_{\text{fermions}} g_i \left(\frac{T_i}{T}\right)^4 \tag{49}$$

where $T$ is the temperature of the plasma. $g_*$ changes with temperature, because, as the temperatures diminish, particles go from a relativistic regime to a non-relativistic one, once their mass is bigger than their temperature. When all the relativistic particles are in equilibrium (i.e. $T_i = T$), $g_* \simeq g_{*s}$, once their contribution to the total entropy in the Universe also depends on their internal number of degrees of freedom. This is the case for the Early Universe, when particles fall out of equilibrium with the plasma soon after they transition to a non-relativistic regime. Hence, for the Standard Model, the effective number of relativistic degrees of freedom can be approached in the same procedure as for $g_{*s}$ [28]:

$$\begin{aligned} g_* = 100,\ T \gtrsim 200\text{MeV} \\ g_* = 10,\ 200\text{MeV} > T \gtrsim 0.1\text{MeV} \\ g_* = 3,\ 0.1\text{MeV} > T \end{aligned} \tag{50}$$

When all the relativistic particles are in equilibrium (i.e. $T_i = T$), $g_* \simeq g_{*s}$, once their contribution to the total entropy in the Universe also depends on their internal number of degrees of freedom. This is the case for the Early Universe, when particles fall out of equilibrium with the plasma soon after they transition to a non-relativistic regime.

With these values of $\rho$ and $g_*$, we can find the values of Hubble rate in this era, through the Friedman Equation:

$$\begin{aligned} H^2 &= \frac{8\pi G}{3}\rho(t) \\ H^2 &= \frac{8\pi G}{3}\frac{\pi^2}{30}g_*(T)T^4 \\ \Rightarrow H &= \sqrt{\frac{8\pi^3 G}{90}g_*(T)}T^2 \end{aligned} \tag{51}$$

Now that we know how the Universe expansion behaved during Dark Matter production, we need to develop a tool to analyse how the DM density changed with time.

## 3. BOLTZMANN EQUATION

If the number of Dark Matter particles were constant in our Universe, then DM number density would diminish proportionally to the Universe expansion, as $n \propto a^{-3}(t)$. However, the total number of DM particles is not constant. It can be modified through different interactions, such as self-annihilation (2 DM particles collide and are destroyed), co-annihilation (the DM particle collides with another particle, and both are destroyed), or the decay of other particles (a new particle, more massive than DM, decays and creates a new DM particle). Therefore, we need a tool to study how such interactions affect the total number density of DM.

In 1872, the Austrian physicist Ludwig Boltzmann published an important paper, where he developed an equation to analyse how the atoms of a diluted gas behave in a system approaching equilibrium. This paper supplied the mathematical basis to describe how the distribution function of a gas changes with time, which also details how the number and energy density of the ensemble operate [29]. Boltzmann's equation assumes [30]:

- The gas' state can be described by a distribution function $f$, that depends on the time and on each particle's position and velocity.
- The system's particles are modeled as small point-like bodies, and their potentials are spherically symmetric.
- The species number density is sufficiently small, thus we can neglect interactions that have three or more components reacting, such as $A + B + C \rightarrow D + E$, with the exception of many-body decays.
- The reaction time between particles is much lower than the total time analysed.

If we consider the Dark Matter number density to be low enough for it to be modeled as a gas, we can use Boltzmann's Equation to analyse how the DM density changes with time.

The evolution of a particle $i$'s number distribution in the $\Lambda CDM$ Model (a flat, isotropic, homogeneous and expanding Universe, where the expansion is accelerating with time) is described by the Boltzmann Equation [31, 32] as:

$$\frac{\partial F_i(p,t)}{\partial t} - Hp\frac{\partial F_i(p,t)}{\partial p} = C_i(F_i, F_j, p) \tag{52}$$

where $F_i(p,t)$ is the number distribution for particle $i$ with momentum $p$, $H$ is the Hubble constant, and $C$ is a collision term that represents all the interactions that can modify the momentum

distribution of particle $i$. This term usually depends on the distributions of other particle species ($j$), which interact with particle $i$.

Multiplying all terms by $p^2$, and integrating:

$$\int \frac{\partial F_i(p,t)}{\partial t} p^2 \frac{dp}{2\pi^2} - \int H p^3 \frac{\partial F_i(p,t)}{\partial p} \frac{dp}{2\pi^2} = \int C_i(F_i, F_j, p) p^2 \frac{dp}{2\pi^2} \tag{53}$$

The second term can be integrated by parts:

$$H \int_0^\infty p^3 \frac{\partial F_i(p,t)}{\partial p} \frac{dp}{2\pi^2} = \frac{H}{2\pi^2} \left[ p^3 F_i(p,t) - \int_0^\infty 3p^2 F_i(p,t) dp \right] \tag{54}$$

$p^3 F_i(p,t)$ vanishes at 0 and $\infty$ [19], so:

$$= \frac{-H}{2\pi^2} \int_0^\infty 3p^2 F_i(p,t) dp \tag{55}$$

turning Eq. 52 into:

$$\int \frac{\partial F_i(p,t)}{\partial t} p^2 \frac{dp}{2\pi^2} + \frac{3H}{2\pi^2} \int_0^\infty p^2 F_i(p,t) dp = \int C_i(F_i, F_j, p) p^2 \frac{dp}{2\pi^2} \tag{56}$$

Given the number distribution $F_i(p,t)$, we can compute the total number density ($n_i(t)$):

$$n_i(t) = \int F_i(p,t) p^2 \frac{dp}{2\pi^2} \tag{57}$$

We can integrate Eq. 57, and obtain [19]:

$$\frac{dn_i}{dt} + 3Hn_i = \int C_i p^2 \frac{dp}{2\pi^2} \tag{58}$$

The left side of Eq. 58 accounts for the expansion of our Universe, while the right side represents the interactions DM participates. The collision term for particle $i$ can usually be split into three terms:

$$C_i = C_{annihilation} + C_{production} + C_{decay} \tag{59}$$

where the contributions for this expression come from the different processes particle $i$ can participate in. A detailed derivation of each term and their contributions to Eq. 58 is given in Appendix A.

The second term on the left hand side of Eq. 58 represents the dilution of the number density $n$ due to the Universe expansion. In the following we will assume the *radiation dominated era*, so

this dilution is determined by the total radiation density. In order to study the changes in density due to the collision terms (right hand side of Eq. 58), it is useful to define the yield:

$$Y_i = \frac{n_i}{s} \tag{60}$$

where $s$ is the entropy density. Since we assume conservation of entropy, $s$ is only effected by the Universe expansion. Hence, by dividing $n$ by another density, we cancel the effects of Universe expansion, and the yield will be proportional to the total number of Dark Matter particles in the Universe. When particle $i$ is in thermal equilibrium ($\Gamma > H$), it's yield is given by:

$$\overline{Y}_i = \frac{\overline{n}_i}{s} \tag{61}$$

in which case we can use the expressions in Eq. 42, Eq. 37 and Eq. 44.

It is also convenient to use a dimensionless parameter to track the evolution of densities. For our purposes we define:

$$x \equiv \frac{m_\chi}{T} \tag{62}$$

Since for $T \gtrsim m_\chi$ ($T \lesssim m_\chi$) the DM particles are relativistic (non-relativistic), values of $x$ less than one correspond to the non-relativistic regime. In particular, we can assume:

$$\begin{gathered} x \leq 2/3\,, \text{ relativistic regime} \\ 2/3 < x \leq 10\,, \text{ semi-relativistic regime} \\ 10 < x\,, \text{ non-relativistic regime} \end{gathered} \tag{63}$$

In addition to the Dark Matter particle, some of the mechanisms we will discuss also assume the existence of a second beyond the Standard Model particle ($Z$), which interacts with DM. In this case the final Boltzmann Equation for the DM and $Z$ are (see Appendix A):

$$\begin{aligned} \frac{dY_\chi}{dx} = \frac{1}{3H}\left|\frac{ds}{dx}\right| \Bigg[ & -\langle\sigma v\rangle_{\chi\chi}(Y_\chi^2 - \overline{Y}_\chi^2) - \langle\sigma v\rangle_{\chi Z}(Y_\chi Y_Z - \overline{Y}_\chi \overline{Y}_Z) + \frac{K_1(m_Z/T)}{K_2(m_Z/T)}\frac{\Gamma_Z}{s}\left(Y_Z - Y_\chi \frac{\overline{Y}_Z}{\overline{Y}_\chi}\right) \\ & + \frac{\Gamma_{Z\to\chi}}{s}\left(Y_Z - \overline{Y}_Z \frac{Y_\chi}{\overline{Y}_\chi}\right) + \langle\sigma v\rangle_{ZZ\to\chi\chi}\left(\frac{Y_Z^2}{\overline{Y}_Z^2} - \frac{Y_\chi^2}{\overline{Y}_\chi^2}\right)\Bigg] \end{aligned} \tag{64}$$

$$\begin{aligned} \frac{dY_Z}{dx} = \frac{1}{3H}\left|\frac{ds}{dx}\right| \Bigg[ & -\langle\sigma v\rangle_{ZZ}(Y_Z^2 - \overline{Y}_Z^2) - \langle\sigma v\rangle_{\chi Z}(Y_\chi Y_Z - \overline{Y}_\chi \overline{Y}_Z) - \frac{K_1(m_Z/T)}{K_2(m_Z/T)}\frac{\Gamma_Z}{s}\left(Y_Z - Y_\chi \frac{\overline{Y}_Z}{\overline{Y}_\chi}\right) \\ & - \frac{\Gamma_{Z\to\chi}}{s}\left(Y_Z - \overline{Y}_Z \frac{Y_\chi}{\overline{Y}_\chi}\right) - \langle\sigma v\rangle_{ZZ\to\chi\chi}\left(\frac{Y_Z^2}{\overline{Y}_Z^2} - \frac{Y_\chi^2}{\overline{Y}_\chi^2}\right)\Bigg] \end{aligned} \tag{65}$$

where $K_n$ are the modified Bessel functions of second kind and $\overline{Y}_i$ are the equilibrium yields, which depends on the $m/T$ ratio and were defined in Eq. 42, Eq. 37 and Eq. 44. The first term in Eq. 64 accounts for self-annihilation of Dark Matter, $\chi + \chi \leftrightarrow SM + SM$, and is illustrated by the diagram Fig. 4.1; the second term represents co-annihilation between $\chi$ and $Z$ (Fig. 4.2), in $\chi + Z \leftrightarrow SM + SM$; the third term corresponds to the decay and inverse decay processes, $Z \leftrightarrow \chi + SM$ (Fig. 4.2); the fourth term represents conversion of $Z$ particles to DM particles through the process $Z+SM \leftrightarrow \chi+SM$ (Fig. 4.4); lastly, the fifth term amounts to the annihilation of $Z$ particles to DM particles, $Z + Z \leftrightarrow \chi + \chi$ (Fig. 4.5).

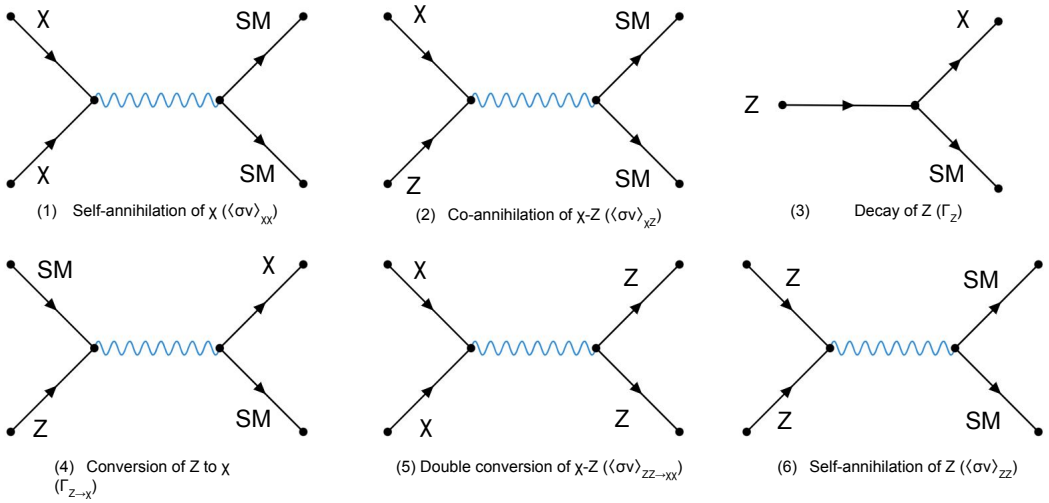


FIG. 4: Feynman diagrams for all the interactions considered for the derivation of Eq. 64 and Eq. 65.

The $ds/dx$ ratio compensate for alterations on $s$, caused by Universe expansion. Using the expression for entropy density in Eq. 45:

$$\frac{ds}{dx} = -\frac{6\pi^2}{45} g_{*s}(x) \frac{m_\chi^3}{x^4} \tag{66}$$

## 4. RESULTS

In this section, we shall analyse different mechanisms for DM production. Our objective is to understand how these models work, what are their suppositions about DM and about the particles it interacts with (in this case, the $Z$ particle), what are their main characteristics, and how they respond when we alter the model's main parameters. We are interested in studying which

mechanisms can supply the abundance of Dark Matter we see today in our Universe, and which constraints they impose in the DM mass and interactions.

For simplicity, in all the results presented here we assume the thermally averaged cross-sections are constant, with constant values of $g_*$ and $g_{*s}$ throughout the production process. We also consider both the DM particle $\chi$ and the $Z$ particle to be fermions, with only one degree of freedom each, for all the cases considered (with the exception of the Conversion-Driven Freeze-Out mechanism, in Sec. 4 4.3, where we take $g_Z = 2$).

### 4.1. Freeze-Out

The simplest model to be considered consists of self-annihilating Dark Matter particles $\chi$ without any other relevant interactions or additional BSM (Beyond the Standard Model) particles. In this case:

$$\langle \sigma v \rangle_{\chi Z} = \Gamma_Z = \Gamma_{Z\to\chi} = \langle \sigma v \rangle_{\chi\chi\to ZZ} = \langle \sigma v \rangle_{ZZ} = 0\,, \tag{67}$$

thus the general Boltzmann Equation, Eq. 64, becomes simply:

$$\frac{dY_\chi}{dx} = -\frac{1}{3H}\left|\frac{ds}{dx}\right| \langle \sigma v \rangle_{\chi\chi}(Y_\chi^2 - \overline{Y}_\chi^2) \tag{68}$$

In addition we consider that, for $T \gg m_\chi$, Dark Matter is in thermal equilibrium with the thermal bath, and therefore its yield follows the equilibrium distribution. For such temperatures DM is relativistic and its self-annihilation cross-section is compensated by the inverse reaction $SM + SM \to \chi + \chi$ [19, 27, 33–38]. A numerical resolution of Eq. 68 is shown in Fig. 5, where it was employed a model with $m_\chi = 700$ GeV, $\langle \sigma v \rangle_{\chi\chi} = \sigma v_{\chi\chi} = 10^{-12}$ GeV$^{-2}$ and the number of degrees of freedom for DM taken as $g_\chi = 1$.

In the freeze-out mechanism, Dark Matter is in thermal equilibrium in early times. In this phase, Dark Matter is relativistic and its yield tracks the equilibrium yield due to the reactions $\chi + \chi \leftrightarrow SM + SM$. As the Universe expands, the temperature decreases and all particles in thermal equilibrium (which we take into account to be Dark Matter and the Standard Model particles) lose kinetic energy. However, for the interaction $SM + SM \to \chi + \chi$ to occur, it is necessary that the Standard Model particles have, at least, $2m_\chi$ of energy. Hence, the Universe expansion will suppress the production rate, since the Standard Model particles do not have enough energy to produce DM. On the other hand, since we assume $m_\chi \gg m_{SM}$, Dark Matter always has enough energy to annihilate into Standard Model particles and the decrease in temperature

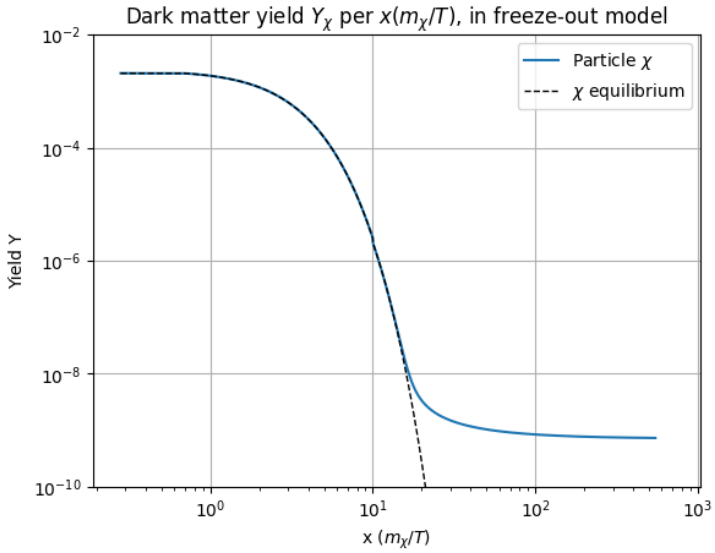


FIG. 5: Dark matter yield (blue) and its equilibrium yield (black), employing a model with $m_\chi = 700$ GeV, $\langle\sigma v\rangle_{\chi\chi} = \sigma v_{\chi\chi} = 10^{-12}$ GeV$^{-2}$ and $g_\chi = 1$.

does not suppress the reaction $\chi + \chi \to SM + SM$. The difference between the self-annihilation and production of Dark Matter rates results in a decline in $Y_\chi$ as $x$ increases (i.e. as temperature declines). This is shown in Fig.5 by the decrease in yield for $x \gtrsim 1$. Note, however, that until $x \simeq 20$, DM still is in thermal equilibrium. The energy suppression of the thermal yield is called *Boltzmann suppression* and follows an exponential distribution, as seen in Eq.44. Finally, at $x \simeq 20$, the DM density is so small that the self-annihilation stops. This results in a constant yield for $\chi$, that has now frozen out. The freeze-out temperature is approximately given by the temperature when the particle reaction rate is smaller than the Hubble rate $H$ (i.e. Universe expansion is separating particles faster than they can react):

$$H(x) \simeq \left|\frac{ds}{dx}\right| \langle\sigma v\rangle_{\chi\chi} \to x_f = \frac{m_\chi}{T_f} \tag{69}$$

It is also possible to obtain an approximate analytical solution to Eq. 68. Since we assume a radiation dominated Universe, the approximation in Eq. 51 is valid for this process:

$$H = \sqrt{\frac{8\pi^3 G}{90} g_*(T)} \left(\frac{m_\chi}{x}\right)^2 \tag{70}$$

Using the above result, along with the $ds/dx$ derivative in Eq. 66, we can integrate Eq. 68:

$$\begin{aligned}\int_{x_0}^{\infty}\frac{1}{Y_\chi^2}\frac{dY_\chi}{dx}dx &= \int_{x_0}^{\infty}-\frac{1}{3H}\left|\frac{ds}{dx}\right|\langle\sigma v\rangle_{\chi\chi}(1-\frac{\overline{Y}_\chi^2}{Y_\chi^2})dx \\ &= -\int_{x_0}^{\infty}\frac{\sqrt{90}x^2}{3\sqrt{8\pi^3 G g_*(x)}m_\chi^2}\frac{6\pi^2}{45}g_{*s}(x)\frac{m_\chi^3}{x^4}\langle\sigma v\rangle_{\chi\chi}(1-\frac{\overline{Y}_\chi^2}{Y_\chi^2})dx \\ &= -\sqrt{\frac{\pi}{45G}}m_\chi\langle\sigma v\rangle_{\chi\chi}\int_{x_0}^{\infty}\frac{g_{*s}(x)}{\sqrt{g_*(x)}}\frac{1}{x^2}(1-\frac{\overline{Y}_\chi^2}{Y_\chi^2})dx \end{aligned} \tag{71}$$

From the above result we see that, while $Y_\chi \simeq \bar{Y}_\chi$, the contribution to the integral is negligible, since the right hand side is zero. Therefore we can take $x_0 = x_f > 1$, where $x_f$ is the point where DM starts to freeze-out (e.g. $x_f \simeq 20$ in Fig.5). As $x$ increases above $x_f$, $\overline{Y}_\chi$ decreases exponentially, as shown in Eq. 44. Hence, if $x_f \gg 1$, we can assume $\overline{Y}_\chi \simeq 0$ for all the integration range. Since the integrand is maximum around $x \simeq x_f$, we can assume most of the contribution to the integral takes place around $x = x_f$. Thus we can assume $g(x) \simeq g(x_f)$ and $g_{*s}(x) \simeq g_{*s}(x_f)$. Under these approximations:

$$\int_{x_f}^{\infty}\frac{1}{Y_\chi^2}\frac{dY_\chi}{dx}dx = -\sqrt{\frac{\pi}{45G}}\frac{g_{*s}(x_f)}{\sqrt{g_*(x_f)}}m_\chi\langle\sigma v\rangle_{\chi\chi}\int_{x_f}^{\infty}\frac{1}{x^2}dx \tag{72}$$

Finally, integrating between $x_f$ and $\infty$:

$$\int_{x_f}^{\infty}\frac{1}{Y_\chi^2}\frac{dY_\chi}{dx} = \frac{1}{Y_\infty}-\frac{1}{Y_f} \approx -\sqrt{\frac{\pi}{45G}}\frac{g_{*s}(x_f)}{\sqrt{g_*(x_f)}}m_\chi\langle\sigma v\rangle_{\chi\chi}\int_{x_f}^{\infty}\frac{1}{x^2}dx = \sqrt{\frac{\pi}{45Gg_*(x_f)}}\frac{g_{*s}(x_f)m_\chi}{x_f}\langle\sigma v\rangle_{\chi\chi} \tag{73}$$

and since $Y_\infty$ is much smaller than $Y_f$, as we can see in Fig. 5, we obtain:

$$Y_\infty \approx \sqrt{\frac{45Gg_*(x_f)}{\pi}}\frac{x_f}{g_{*s}(x_f)m_\chi\langle\sigma v\rangle_{\chi\chi}} \tag{74}$$

Applying this result for the model shown in Fig. 5, we obtain $Y_\infty \approx 7.52\times10^{-10}$, whereas the numerical result is $Y_\chi = 7.25\times10^{-10}$, which shows a good agreement between both methods. The difference between both results is caused by the assumption that $\overline{Y}_\chi$ can be neglected in the whole interval of integration. In reality, $\overline{Y}_\chi$ is not excessively smaller than $Y_\chi$ around $x = x_f$, which yields a 3% error in the analytical solution.

It is also interesting to investigate how the final yield is affected by different choices of model parameters. According to Eq. 74, we can conclude that increasing the cross section $\langle\sigma v\rangle_{\chi\chi}$ will reduce the final yield of Dark Matter, as can be seen in Fig. 6. Physically, increasing the cross section means that the particle will interact with a higher reaction rate. In the case of freeze-out, the interactions are annihilating Dark Matter, hence an increase in the cross section will result in

a smaller final yield. It is also interesting to notice that the different values of cross section lead to different values of $x_f$, the value of $x$ when the freeze-out process begins. This is expected, since larger cross-sections will delay the freeze-out and therefore increase the value of $x_f$.

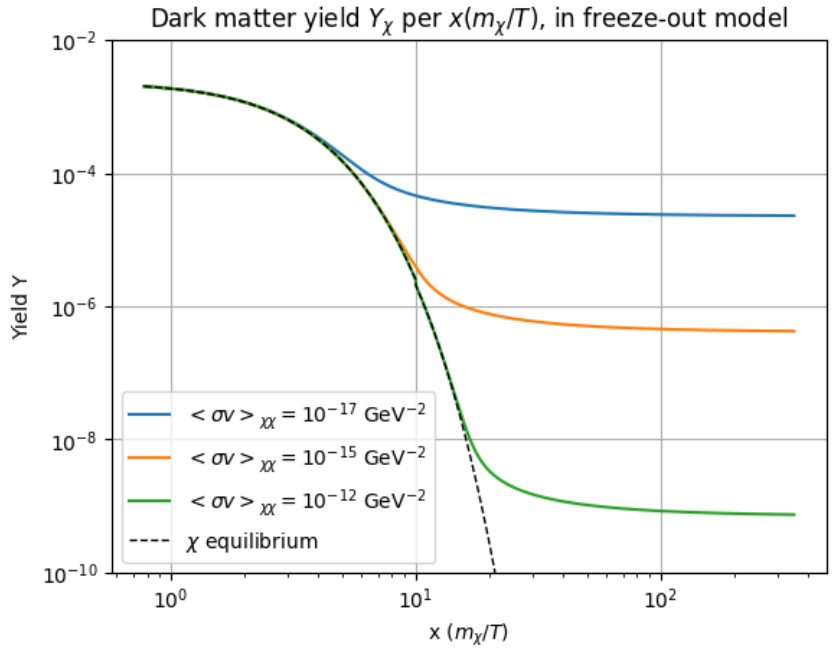


FIG. 6: Dark matter yield for different values of self-annihilation cross section. The other parameters are the same used in Fig.5.

Changing the value of the DM mass will also impact its final yield, as seen in Fig. 7. With a higher mass, Standard Model particles will need more energy to produce Dark Matter through $SM + SM \rightarrow \chi + \chi$, which makes this reaction less likely. This reduction in the production of DM through $SM + SM \rightarrow \chi + \chi$ rate leads $Y_\chi$ to decrease faster, which can be seen numerically by noticing the effect of the mass in its non-relativistic equilibrium expectancy (Eq. 44). Therefore, when the Universe expansion separates DM particles and causes them to stop reacting, there will be less particles, thus a lower final yield.

Note that, in Fig. 7, we have changed our horizontal axis to $700\text{GeV}/T$, since we have assumed different mass values.

In order to compare the values obtained to the Dark Matter energy density measured experimentally, we can compute the DM relic density using the final yield value. According to the $\Lambda CDM$ Model, Dark Matter must have low velocities today, therefore we can approach that its


FIG. 7: Dark matter yield for different mass values, in a freeze-out model. The other parameters are the same used in Fig.5.

total energy is well approached by its rest energy:

$$\begin{aligned} \rho_\chi(t) &= n_\chi(t) m_\chi = Y_\infty s(t_0) m_\chi \\ \Rightarrow \Omega_\chi h^2 &= \frac{\rho_\chi}{\rho_c} = \frac{s(t_0) m_\chi}{\rho_c} Y_\infty \end{aligned} \tag{75}$$

where $\rho_c = 4.79 \times 10^{-6}$ GeV cm$^{-3}$ is the critical density and $s(t_0) = 2891.2$ cm$^{-3}$ is the entropy density today [1]. Using our approximation for $Y_\infty$ in Eq. 74 we obtain:

$$\Omega_\chi h^2 = \frac{\rho_\chi}{\rho_c} = \frac{s m_\chi}{\rho_c} \sqrt{\frac{45 G g_*(x_f)}{\pi}} \frac{x_f}{g_{*s(x_f)} m_\chi \langle \sigma v \rangle_{\chi\chi}} \simeq 1.871 \times 10^{-11} \frac{x_f}{\langle \sigma v \rangle_{\chi\chi}} \tag{76}$$

If we compare the above result with recent observations of the DM relic abundance[1] ($\Omega_\chi^{\rm obs} h^2 = 0.12$) and assuming $x_f \simeq 20$, we have:

$$\langle \sigma v \rangle_{\chi\chi} \approx 3.12 \times 10^{-9} \text{GeV}^{-2} \tag{77}$$

This result is known as the 'WIMP Miracle', since the cross section value is similar to electroweak cross sections, which has been interpreted as a hint that WIMPs (Weakly-Interacting Massive Particles), generated through freeze-out, are a good Dark Matter candidate. Also, many models provide candidates with cross sections in this range [39].

The freeze-out mechanism is also attractive because, as Dark Matter is in thermal equilibrium in early times, the process and the final yield do not depend on external factors prior to the freeze-out, as inflation and reheating processes. It also guarantees that Dark Matter will be sufficiently cold to allow for cosmological structure formation [40].

Since this discovery in the 1990s, many types of detectors have been built to search for Dark Matter, using different strategies of detection. Some examples of detectors are DAMA/LIBRA II, COSSINE-100, XENON100, LUX, PICASSO, among others. However, until the present moment, there have not been any evidences found for WIMP Dark Matter from these detectors [41].

### 4.2. WIMPs with co-annihilation

A different type of freeze-out can take place when we add a second particle species ($Z$), which can co-annihilate with Dark Matter ($\chi$) through the process $\chi + Z \to SM + SM$. This model considers $Z$ to be almost degenerate in mass with DM, $m_Z \gtrsim m_\chi$ [42–48]. In this mechanism we also assume that $Z$ and $\chi$ have large self-annihilation cross-sections. If the mass difference, $\Delta m \equiv (m_Z - m_\chi)$, is much larger than the DM freeze-out temperature ($T_f$), co-annihilation will not influence the Dark Matter freeze-out. If $m_Z \gg m_\chi$, particle $Z$ will freeze-out much earlier than DM, and the co-annihilated $\chi$ particles will be restored by the process $SM + SM \to \chi + \chi$, which is still occurring efficiently during $Z$ freeze-out. Hence, when DM falls out of equilibrium, there is very few $Z$ particles for it to react with.

The main reactions for the co-annihilation mechanism are $\chi + \chi \leftrightarrow SM + SM$ (self-annihilation of Dark Matter), $Z + Z \leftrightarrow SM + SM$ (self-annihilation of $Z$), $\chi + Z \leftrightarrow SM + SM$ (co-annihilation), $Z \leftrightarrow \chi + SM + SM$ (three body decay of $Z$) and $Z + SM \leftrightarrow \chi + SM$ (conversion). The three body decay of $Z$ and the conversion reactions are available interactions in this model because they are closely related to the co-annihilation process, as can be seen in Fig. 4. Nonetheless, the decay process $Z \leftrightarrow \chi + SM + SM$ will be suppressed due to the small mass difference $\Delta m$, and the conversion reaction will be suppressed when $Y_\chi \simeq Y_Z$.

Under the previous assumptions, this model corresponds to:

$$\langle \sigma v \rangle_{\chi\chi} \simeq \langle \sigma v \rangle_{ZZ} \gg \langle \sigma v \rangle_{\chi\chi \to ZZ}, \text{ and } m_\chi \simeq m_Z \tag{78}$$

turning Boltzmann Equation into:

$$\frac{dY_\chi}{dx} = \frac{1}{3H}\left|\frac{ds}{dx}\right|\left[-\langle\sigma v\rangle_{\chi\chi}(Y_\chi^2 - \overline{Y}_\chi^2) - \langle\sigma v\rangle_{\chi Z}(Y_\chi Y_Z - \overline{Y}_\chi\overline{Y}_Z)\right.$$
$$\left. + \frac{K_1(m_Z/T)}{K_2(m_Z/T)}\frac{\Gamma_Z}{s}\left(Y_Z - Y_\chi\frac{\overline{Y}_Z}{\overline{Y}_\chi}\right) + \frac{\Gamma_{Z\to\chi}}{s}\left(Y_Z - \overline{Y}_Z\frac{Y_\chi}{\overline{Y}_\chi}\right)\right], \tag{79}$$

$$\frac{dY_Z}{dx} = \frac{1}{3H}\left|\frac{ds}{dx}\right|\left[-\langle\sigma v\rangle_{ZZ}(Y_Z^2 - \overline{Y}_Z^2) - \langle\sigma v\rangle_{\chi Z}(Y_\chi Y_Z - \overline{Y}_\chi\overline{Y}_Z)\right.$$
$$\left. - \frac{K_1(m_Z/T)}{K_2(m_Z/T)}\frac{\Gamma_Z}{s}\left(Y_Z - Y_\chi\frac{\overline{Y}_Z}{\overline{Y}_\chi}\right) - \frac{\Gamma_{Z\to\chi}}{s}\left(Y_Z - \overline{Y}_Z\frac{Y_\chi}{\overline{Y}_\chi}\right)\right] \tag{80}$$

Choosing a model with $m_\chi = 700$ GeV, $m_Z = 710$ GeV, $\langle\sigma v\rangle_{\chi\chi} = 10^{-16}\text{GeV}^{-2}$, $\langle\sigma v\rangle_{\chi Z} = 10^{-15}\text{GeV}^{-2}$, $\langle\sigma v\rangle_{ZZ} = 10^{-15}\text{GeV}^{-2}$, $\Gamma_Z = 10^{-16}$ GeV, $\Gamma_{Z\to\chi} = 10^{-15}$ GeV, and $g_\chi = g_Z = 1$, we obtain the results shown in Fig. 8. In this figure, we consider a model without co-annihilation (i.e. $\langle\sigma v\rangle_{\chi Z} = \Gamma_{Z\to\chi} = 0$), for comparison. To account for a better comparison, we consider that, in the model without co-annihilation, there is a two body decay of $Z$ ($Z \to \chi + SM$), with the same decay width as the three body decay in the model with co-annihilation. Thus, $Z$ will decay in both models, with the same reaction rate. In Eq. A14, we note that adding a new SM particle to the Feynman diagram of the decay will not alter the expression in the Boltzmann Equation, once SM particles are in thermal equilibrium, which implies $n_{SM}/\overline{n}_{SM} = 1$.

In this mechanism, both particles are in thermal equilibrium at early times. As the Universe expands, its temperature declines, causing all particles in the thermal bath (which we consider to be the Standard Model particles, DM and $Z$) to lose kinetic energy. Hence, the SM particles do not have enough energy to interact as $SM+SM \to \chi+\chi$, $SM+SM \to Z+Z$, and $SM+SM \to \chi+Z$, once we assumed $m_Z \gtrsim m_\chi \gg m_{SM}$. Thus, these reactions rates will be suppressed. On the other hand, $\chi$ and $Z$ always have enough energy to react, due to their mass difference with the SM particles, and therefore the self-annihilation reactions and the co-annihilation reaction continue to occur at the same rate. The contrast between DM and $Z$ production and annihilation leads to a decline in $Y_\chi$ and $Y_Z$ (i.e. $Y_\chi$ and $Y_Z$ become Boltzmann suppressed), following their equilibrium values. Due to the small mass gap between Dark Matter and $Z$, their equilibrium yields are fairly close, leading to $Y_\chi \simeq Y_Z$ before $x \simeq 9$.

Around $x \simeq 9$, both Dark Matter and $Z$ begin to decouple from the thermal bath, following a freeze-out pattern. The difference between their self-annihilation cross sections $\langle\sigma v\rangle_{\chi\chi}$ and $\langle\sigma v\rangle_{ZZ}$ causes a contrast in their yields, with $Y_\chi > Y_Z$ in $x \simeq 10$. This contrast enhances conversion reactions $\chi + SM \to Z + SM$ and inverse decays $\chi + SM \to Z$, reducing $Y_\chi$. The produced $Z$ particles create a bump in $Y_Z$, around $x \simeq 40$. In the model without co-annihilation, the bump in

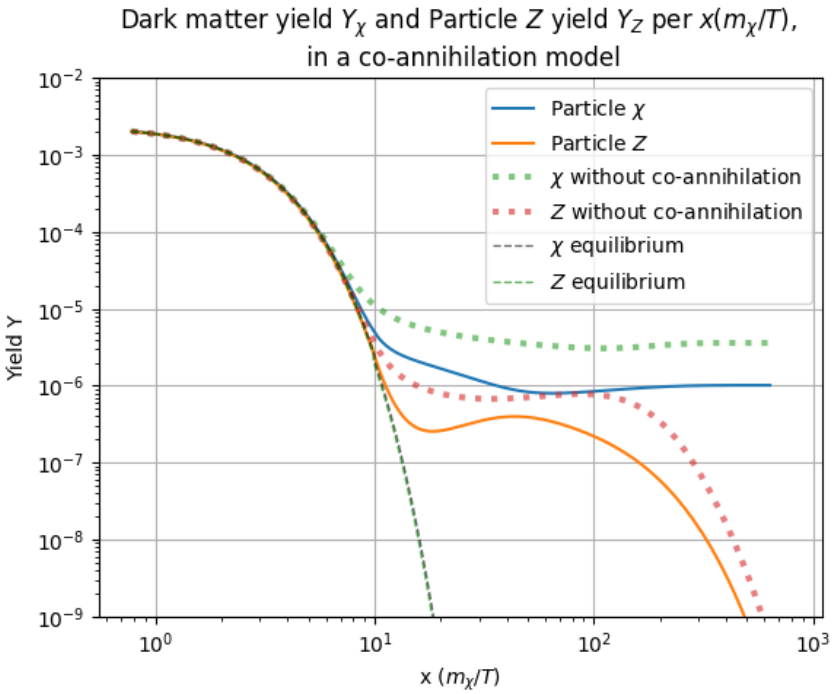


FIG. 8: Dark matter yield (blue) and particle $Z$ yield (orange), along with their equilibrium yields, in a co-annihilation model. The dotted lines represent the respective yields if co-annihilation reaction was neglected (i.e. $\langle\sigma v\rangle_{\chi Z} = \Gamma_{Z\to\chi} = 0$). The graph used a model with $m_\chi = 700$ GeV, $m_Z = 710$ GeV, $\langle\sigma v\rangle_{\chi\chi} = 10^{-16}\text{GeV}^{-2}$, $\langle\sigma v\rangle_{\chi Z} = 10^{-15}\text{GeV}^{-2}$, $\langle\sigma v\rangle_{ZZ} = 10^{-15}\text{GeV}^{-2}$, $\Gamma_Z = 10^{-16}$ GeV, $\Gamma_{Z\to\chi} = 10^{-15}$ GeV, and $g_\chi = g_Z = 1$.

the $Z$ yield is caused solely by the inverse decays, once the conversion interaction is not available in this model. Eventually, $Z$ begins to decay in both models, and DM yield is enlarged lightly.

As done in the case of freeze-out, we can find an analytical solution for this model. It is convenient to define [42]:

$$\Delta_Z = \frac{m_Z - m_\chi}{m_\chi} \tag{81}$$

We work with the assumption that [42, 49]:

$$\frac{Y_i}{Y_\text{T}} \simeq \frac{\overline{Y}_i}{\overline{Y}_\text{T}} \tag{82}$$

where $Y_T \equiv Y_\chi + Y_Z$, and $\overline{Y}_T \equiv \overline{Y}_\chi + \overline{Y}_Z$.

Using the expressions for the equilibrium yields in the non-relativistic regime (Eq.44), we have:

$$\frac{\overline{Y}_i}{\overline{Y}_\text{T}} = \frac{(m_i/m_\chi)^{3/2}\exp(-m_i/T)}{\exp(-m_\chi/T) + (m_Z/m_\chi)^{3/2}\exp(-m_Z/T)} \tag{83}$$

The expression $m_i/m_\chi$ can be rewritten as:

$$\frac{m_i}{m_\chi} = \frac{m_i - m_\chi + m_\chi}{m_\chi} = \frac{m_i - m_\chi}{m_\chi} + 1 = \Delta_i + 1 \tag{84}$$

Hence:

$$\frac{\overline{Y}_i}{\overline{Y}_\mathrm{T}} = \frac{(1+\Delta_i)^{3/2}\exp(-m_i/T)}{\exp(-m_\chi/T) + (1+\Delta_Z)^{3/2}\exp(-m_Z/T)} \tag{85}$$

Subsequently, multiplying all terms by $\exp(m_\chi/T)$:

$$\frac{\overline{Y}_i}{\overline{Y}_\mathrm{T}} = \frac{(1+\Delta_i)^{3/2}\exp((-m_i + m_\chi)/T)}{1 + (1+\Delta_Z)^{3/2}\exp((-m_Z + m_\chi)/T)} \tag{86}$$

and using

$$\frac{-m_i + m_\chi}{T} = \frac{-(m_i - m_\chi)x}{m_\chi} = -\Delta_i x \tag{87}$$

we obtain

$$\frac{\overline{Y}_i}{\overline{Y}_\mathrm{T}} = \frac{(1+\Delta_i)^{3/2}\exp((-\Delta_i x)}{g_{eff}} \tag{88}$$

where:

$$g_{eff} = 1 + (1+\Delta_Z)^{3/2}\exp(-\Delta_Z x) \tag{89}$$

The analytical solution to $Y_\chi$ can be further simplified if we consider the differential equation for the total yield ($Y_\mathrm{T}$):

$$\frac{dY_T}{dx} = \frac{1}{3H}\left|\frac{ds}{dx}\right|\left[-\langle\sigma v\rangle_{\chi\chi}(Y_\chi^2 - \overline{Y}_\chi^2) - 2\langle\sigma v\rangle_{\chi Z}(Y_\chi Y_Z - \overline{Y}_\chi \overline{Y}_Z) - \langle\sigma v\rangle_{ZZ}(Y_Z^2 - \overline{Y}_Z^2)\right] \tag{90}$$

We can now use Eqs. 82 and 88 to write:

$$\begin{gathered} Y_\chi = \frac{\overline{Y}_\chi Y_T}{\overline{Y}_T}\ ,\ Y_Z = \frac{\overline{Y}_Z Y_T}{\overline{Y}_T} \\ \overline{Y}_\chi = \frac{1}{g_{eff}}\overline{Y}_T\ ,\ \overline{Y}_Z = \frac{(1+\Delta_Z)^{3/2}\exp(-x\Delta_Z)}{g_{eff}}\overline{Y}_T \end{gathered} \tag{91}$$

and obtain:

$$\begin{aligned} \frac{dY_T}{dx} = \frac{1}{3H}\left|\frac{ds}{dx}\right|\Bigg[&-\langle\sigma v\rangle_{\chi\chi}\left(\left(\frac{\overline{Y}_\chi Y_T}{\overline{Y}_T}\right)^2 - \left(\frac{\overline{Y}_T}{g_{eff}}\right)^2\right) \\ &-2\langle\sigma v\rangle_{\chi Z}\left(\left(\frac{\overline{Y}_\chi Y_T}{\overline{Y}_T}\frac{\overline{Y}_Z Y_T}{\overline{Y}_T}\right) - \left(\frac{g_\chi \overline{Y}_T}{g_{eff}}\frac{(1+\Delta_Z)^{3/2}\exp(-x\Delta_Z)\overline{Y}_T}{g_{eff}}\right)\right) \\ &-\langle\sigma v\rangle_{ZZ}\left(\left(\frac{\overline{Y}_Z Y_T}{\overline{Y}_T}\right)^2 - \left(\frac{(1+\Delta)^{3/2}\exp(-x\Delta)\overline{Y}_T}{g_{eff}}\right)^2\right)\Bigg] \end{aligned} \tag{92}$$

Then, using our expression for $\overline{Y}_i/\overline{Y}_T$ from Eq. 88:

$$\frac{dY_T}{dx} = \frac{1}{3H}\left|\frac{ds}{dx}\right|\left[-\langle\sigma v\rangle_{\chi\chi}\left(\left(\frac{1}{g_{eff}}Y_T\right)^2 - \left(\frac{1\overline{Y}_T}{g_{eff}}\right)^2\right)\right.$$
$$-2\langle\sigma v\rangle_{\chi Z}\left(\left(\frac{1}{g_{eff}}\frac{(1+\Delta_Z)^{3/2}\exp(-x\Delta_Z}{g_{eff}}Y_T^2\right) - \left(\frac{1}{g_{eff}}\frac{(1+\Delta_Z)^{3/2}\exp(-x\Delta_Z)}{g_{eff}}\overline{Y}_T^2\right)\right) \quad (93)$$
$$\left.-\langle\sigma v\rangle_{ZZ}\left(\left(\frac{(1+\Delta_Z)^{3/2}\exp(-x\Delta_Z)}{g_{eff}}Y_T^2\right)^2 - \left(\frac{(1+\Delta_Z)^{3/2}\exp(-x\Delta_Z)\overline{Y}_T}{g_{eff}}\right)^2\right)\right]$$

Finally we can rewrite the above result as:

$$\frac{dY_T}{dx} = -\frac{1}{3H}\left|\frac{ds}{dx}\right|\langle\sigma_{eff}v\rangle(Y_T^2 - \overline{Y}_T^2) \quad (94)$$

where:

$$\sigma_{eff} \equiv \sigma_{\chi\chi}\frac{1}{g_{eff}^2} + 2\sigma_{\chi Z}\frac{1}{g_{eff}^2}(1+\Delta_Z)^{3/2}\exp(-x\Delta_Z) + \sigma_{ZZ}\frac{1}{g_{eff}^2}(1+\Delta_Z)^3\exp(-2\Delta_Z x) \quad (95)$$

The result in Eq. 94 allows us to rewrite the co-annihilation process as a freeze-out process for the total $(Z+\chi)$ yield. Since after $Z$ decays, its yield is converted to DM, the total yield corresponds to the final DM yield. It is also interesting to notice that, if $\Delta_Z \gg 1$, the last two terms in Eq.95 are suppressed (remember that $x > 1$ during freeze-out) and we have the usual freeze-out mechanism.

Expanding $\sigma_{eff}$ on $\Delta_Z$ using a Taylor series:

$$\sigma_{eff} = \frac{1}{4}(\sigma_{\chi\chi} + 2\sigma_{\chi Z} + \sigma_{ZZ}) + \frac{(2x-3)}{8}\Delta_Z(\sigma_{\chi\chi} - \sigma_{ZZ}) \quad (96)$$

Which can be substituted in Eq. 94:

$$\frac{dY_T}{dx} = -\frac{1}{3H}\left|\frac{ds}{dx}\right|\left[\frac{1}{4}(\sigma_{\chi\chi} + 2\sigma_{\chi Z} + \sigma_{ZZ}) + \frac{(2x-3)}{8}\Delta_Z(\sigma_{\chi\chi} - \sigma_{ZZ})\right](Y_T^2 - \overline{Y}_T^2) \quad (97)$$

We can now directly use the freeze-out result (Eq.72) with $\langle\sigma v\rangle_{\chi\chi}$ replaced by $\sigma_{eff}$:

$$\int_{x_f}^{\infty}\frac{1}{Y_T^2}\frac{dY_T}{dx}dx = -\sqrt{\frac{\pi}{45G}}\frac{g_{*s}(x_f)}{\sqrt{g_*(x_f)}}m_\chi\int_{x_f}^{\infty}\sigma_{eff}\frac{1}{x^2}dx \quad (98)$$

Since the maximum of the integrand is at $x = x_f$, we can approach that most of the contribution to the integral occurs around this point. Therefore, we can use the freeze-out result (Eq. 74) with

$\langle\sigma v\rangle_{\chi\chi}$ substituted by $\sigma_{eff}(x_f)$:

$$
\begin{aligned}
Y_\infty &\approx \sqrt{\frac{45Gg_*(x_f)}{\pi}}\frac{x_f}{g_{*s}(x_f)m_\chi\sigma_{eff}(x_f)} \\
&= \sqrt{\frac{45Gg_*(x_f)}{\pi}}\frac{x_f}{g_{*s}(x_f)m_\chi}\left[\frac{1}{4}(\sigma_{\chi\chi}+2\sigma_{\chi Z}+\sigma_{ZZ})+\frac{(2x_f-3)}{8}\Delta_Z(\sigma_{\chi\chi}-\sigma_{ZZ})\right]^{-1} \\
&= 3.1\times10^{-20}\frac{x_f}{m_\chi}\left[\frac{1}{4}(\sigma_{\chi\chi}+2\sigma_{\chi Z}+\sigma_{ZZ})+\frac{(2x_f-3)}{8}\Delta_Z(\sigma_{\chi\chi}-\sigma_{ZZ})\right]^{-1}
\end{aligned}
\tag{99}
$$

For the model in Fig. 8, the analytical approximation gives $Y_\infty \simeq 1.04\times10^{-6}$, which is pretty close to the numerical result $Y_\infty = 1.01\times10^{-6}$. The difference between these numbers can be attributed to the assumption that all the contribution of $\sigma_{eff}$ occurs at $x = x_f$.

The final Dark matter relic abundance then becomes:

$$
\Omega_\chi h^2 = 1.871\times10^{-11}\left[\frac{1}{4}(\sigma_{\chi\chi}+2\sigma_{\chi Z}+\sigma_{ZZ})+\frac{(2x_f-3)}{8}\Delta_Z(\sigma_{\chi\chi}-\sigma_{ZZ})\right]^{-1} \tag{100}
$$

As mentioned previously, co-annihilation will not have an effect on Dark Matter behaviour if $\Delta m \gg T_f$, where $T_f$ is the temperature when DM freezes out. In order to confirm this statement, we shall compare how altering the value of $m_Z$ modifies both yields. In Fig. 9 (left), by increasing $m_Z$, we note that $Y_\chi$ becomes larger after DM decouples from the thermal bath, at $x \simeq 10$, approaching the model without co-annihilation. Therefore, as $\Delta m$ increases, the effect of co-annihilation on DM yield lessens, confirming our previous assumption. Subsequently to the freeze-out, DM density is increased due to $Z$ decay. We also note that, for higher values of $\Delta_Z$, DM particles will need more energy to convert as $\chi + SM \to Z + SM$, or to react as $\chi + SM \to Z$. Therefore, these reactions are suppressed for higher values of $m_Z$.

On the other hand, we note that increasing $m_Z$ causes its yield to be Boltzmann suppressed sooner, while it remains in thermal equilibrium. It also leads to the decay of $Z$ to occur earlier. We remark that, for larger values of $m_Z$, the acceleration of the Boltzmann suppression leads to a smaller value of $Y_Z$ when it decouples from the thermal bath, at $x \simeq 10$. Thus, when $Z$ decays, it produces less DM particles. This is in accordance with the analytical expression obtained in Eq. 99.

Lastly, in Fig. 10, we see show how altering the value of co-annihilation cross section $\langle\sigma v\rangle_{\chi Z}$ changes the final yield of both particles. A lower co-annihilation cross section implies that the co-annihilation reaction will occur less often, therefore diluting less DM particles. Thus, the lower the co-annihilation cross section, the larger the final yield of DM. The same pattern can be seen for $Z$, with a larger cross section leading to a lower yield after decoupling from the thermal bath.

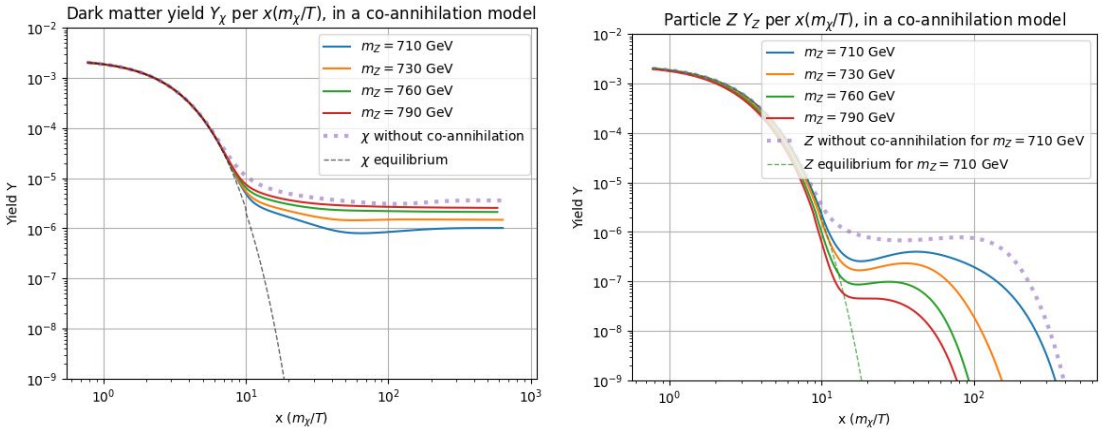


FIG. 9: Dark matter yield $Y_\chi$ (left) and particle $Z$ yield $Y_Z$ (right), in a co-annihilation model, for different values of $m_Z$. The dotted lines represent the respective yields if co-annihilation reaction was neglected (i.e. $\langle\sigma v\rangle_{\chi Z} = \Gamma_Z = \Gamma_{Z\to\chi} = 0$). The model used $m_\chi = 700$ GeV, $\langle\sigma v\rangle_{\chi\chi} = 10^{-16}\text{GeV}^{-2}$, $\langle\sigma v\rangle_{\chi Z} = 10^{-15}\text{GeV}^{-2}$, $\langle\sigma v\rangle_{ZZ} = 10^{-15}\text{GeV}^{-2}$, $\Gamma_Z = 10^{-16}$ GeV, $\Gamma_{Z\to\chi} = 10^{-15}$ GeV, and $g_\chi = g_Z = 1$.

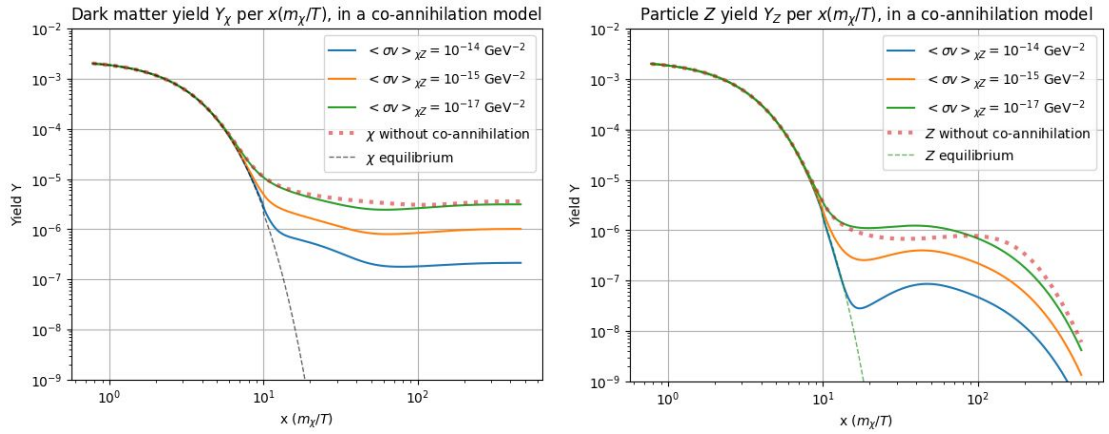


FIG. 10: Dark matter yield $Y_\chi$ (left) and particle $Z$ yield $Y_Z$ (right), in a co-annihilation model, for different values of $\langle\sigma v\rangle_{\chi Z}$. The model used $m_\chi = 700$ GeV, $m_Z = 710$ GeV, $\langle\sigma v\rangle_{\chi\chi} = 10^{-16}\text{GeV}^{-2}$, $\langle\sigma v\rangle_{ZZ} = 10^{-15}\text{GeV}^{-2}$, $\Gamma_Z = 10^{-16}$ GeV, $\Gamma_{Z\to\chi} = 10^{-15}$ GeV, and $g_\chi = g_Z = 1$.

### 4.3. Conversion-Driven Freeze-Out

A new mechanism can take place if we consider the Dark Matter coupling to the Standard Model to be relatively small, leading Dark Matter self-annihilation to be subdominant. In this scenario, Dark Matter is in thermal equilibrium at early times, and the reaction responsible to dilute its

yield is $\chi + SM \to Z + SM$ conversions. In the literature, this is called the Conversion-Driven Freeze-Out (CDFO), also known as co-scattering [40, 50–54].

In this mechanism, the reactions that take a significant role are $Z + Z \leftrightarrow SM + SM$ (self-annihilation of $Z$), $Z + SM \leftrightarrow \chi + SM$ (conversion), $\chi + \chi \leftrightarrow SM + SM$ (self-annihilation of Dark Matter), and $Z \leftrightarrow \chi + SM$ ($Z$ decay). Although the co-annihilation ($Z + \chi \leftrightarrow SM + SM$) cross-section is also large in this model, since it is related to the conversion reaction, the co-annihilation rate is suppressed with respect to the conversion rate due to the small $Z$ densities, as it will be shown later. In our work, we consider that the only particle from the dark sector that interacts with Dark Matter is $Z$, that is more massive than $\chi$ and is also in thermal equilibrium at early times. The implementation of CDFO assumes the following:

$$\begin{aligned} \langle \sigma v \rangle_{ZZ \to \chi\chi} &= 0 \\ \langle \sigma v \rangle_{\chi\chi} &\ll \frac{\Gamma_{Z\to\chi}}{s} \\ m_Z &\gtrsim m_\chi \gg m_{SM} \end{aligned} \tag{101}$$

As a result, the general Boltzmann Equation is reduced to:

$$\begin{aligned} \frac{dY_\chi}{dx} = \frac{1}{3H}\left|\frac{ds}{dx}\right| \Big[ &-\langle \sigma v \rangle_{\chi\chi}(Y_\chi^2 - \overline{Y}_\chi^2) - \langle \sigma v \rangle_{\chi Z}(Y_\chi Y_Z - \overline{Y}_\chi \overline{Y}_Z) \\ &+ \frac{K_1(x)}{K_2(x)}\frac{\Gamma_Z}{s}\left(Y_Z - Y_\chi \frac{\overline{Y}_Z}{\overline{Y}_\chi}\right) + \frac{\Gamma_{Z\to\chi}}{s}\left(Y_Z - \overline{Y}_Z \frac{Y_\chi}{\overline{Y}_\chi}\right)\Big] , \end{aligned} \tag{102}$$

$$\begin{aligned} \frac{dY_Z}{dx} = \frac{1}{3H}\left|\frac{ds}{dx}\right| \Big[ &-\langle \sigma v \rangle_{ZZ}(Y_Z^2 - \overline{Y}_Z^2) - \langle \sigma v \rangle_{\chi Z}(Y_\chi Y_Z - \overline{Y}_\chi \overline{Y}_Z) \\ &- \frac{K_1(x)}{K_2(x)}\frac{\Gamma_Z}{s}\left(Y_Z - Y_\chi \frac{\overline{Y}_Z}{\overline{Y}_\chi}\right) - \frac{\Gamma_{Z\to\chi}}{s}\left(Y_Z - \overline{Y}_Z \frac{Y_\chi}{\overline{Y}_\chi}\right)\Big] \end{aligned} \tag{103}$$

Employing a model with $m_\chi = 500$ GeV, $m_Z = 510$ GeV, $\langle \sigma v \rangle_{\chi\chi} = 10^{-40}$ GeV$^{-2}$, $\Gamma_{Z\to\chi} = 10^{-14}$ GeV, $\Gamma_Z = 10^{-15}$ GeV, $\langle \sigma v \rangle_{ZZ} = 10^{-13}$ GeV$^{-2}$, $g_\chi = 1$ and $g_Z = 2$, we obtain Fig. 11.

As we can see, at early times both particles are in thermal equilibrium. Around $x \simeq 1$ Dark Matter starts to decouple from the thermal bath, due to its small self-annihilation cross-section. In contrast, $Z$ remains in thermal equilibrium even for temperatures below their mass, where its yield starts to become Boltzmann suppressed. At $x \sim 3$, we see that $Y_Z = \bar{Y}_Z$ and $Y_\chi \gg \bar{Y}_\chi$, since Dark Matter has already decoupled. Note that, while $Z$ is in thermal equilibrium, the conversion term in Eq. 102 can be written as:

$$\frac{\Gamma_{Z\to\chi}}{s}\left(\overline{Y}_Z - Y_\chi \frac{\overline{Y}_Z}{\overline{Y}_\chi}\right) = \frac{\Gamma_{Z\to\chi}}{s}\overline{Y}_Z\left(1 - \frac{Y_\chi}{\overline{Y}_\chi}\right) \tag{104}$$

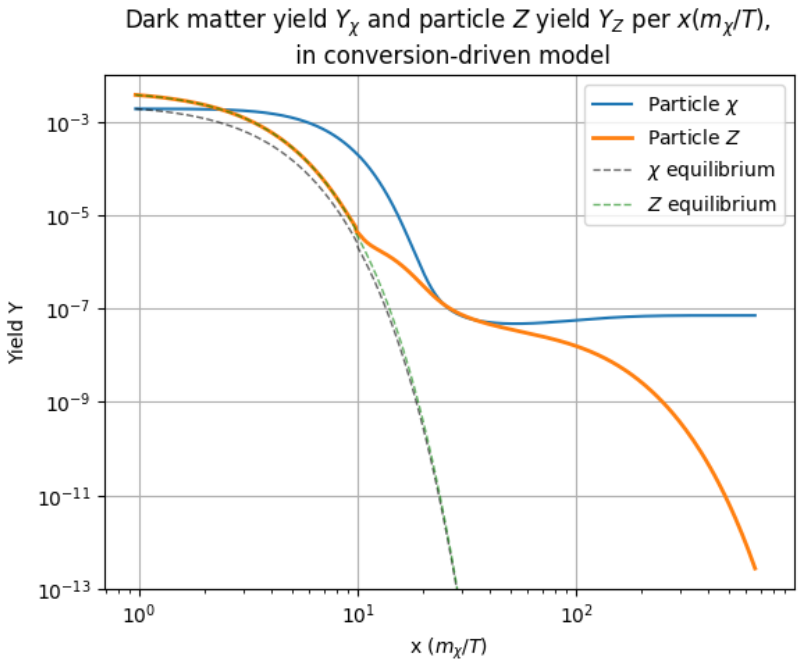


FIG. 11: Dark matter yield $Y_\chi$ (blue) and particle $Z$ yield $Y_Z$ (orange), along with their equilibrium yields, for the conversion-driven freeze-out mechanism. The model used $m_\chi = 500$ GeV, $m_Z = 510$ GeV, $\langle\sigma v\rangle_{\chi\chi} = 10^{-40}\text{GeV}^{-2}$, $\Gamma_Z = 10^{-15}$ GeV, $\Gamma_{Z\to\chi} = 10^{-14}$ GeV, $\langle\sigma v\rangle_{ZZ} = 10^{-13}\text{GeV}^{-2}$, $g_\chi = 1$ and $g_Z = 2$.

As the Dark Matter yield deviates from its equilibrium, the ratio $Y_\chi/\overline{Y}_\chi$ becomes bigger. This difference will enhance $\chi + SM \to Z + SM$ conversions, reducing $Y_\chi$. The $Z$ particles produced in this process will rapidly self-annihilate, keeping the $Z$ density equal to its thermal equilibrium value.

Once the temperature drops even further, at around $x \simeq 10$, due to the small $Z$ yield, the self-annihilation rate ($Z+Z \to SM+SM$) becomes smaller than conversion rate ($\chi+SM \to Z+SM$). The production of $Z$ through $\chi + SM \to Z + SM$ becomes more significant, and $Y_Z$ deviates from its equilibrium value. Finally, at $x \simeq 30$, the conversion process stops once $Y_Z \simeq Y_\chi$, since $\bar{Y}_\chi \simeq \bar{Y}_Z$. Also around this temperature $Z$ starts to decay and its density is converted to Dark Matter, which becomes constant after most of the $Z$ particles have decayed, around $x \sim 300$.

As done to the previous cases, we shall compare how the change in parameters of the model will affect the behaviour of both particles. In Fig. 12, we see a comparison between different mass values for $Z$. First we note that the bigger the value of $m_Z$, the faster will be its Boltzmann suppression while it remains in thermal equilibrium. Also, a larger mass gap between $\chi$ and $Z$ requires more energy for Dark Matter to produce $Z$ through the conversion process $\chi + SM \to Z + SM$. As

a result, the conversion rate is suppressed with respect to the case shown in Fig. 11. A smaller conversion rate means that fewer Dark Matter particles will be converted to $Z$, which means larger values for the final Dark Matter yield, as seen in Fig. 12 (left). In addition, the decoupling of $Z$ becomes closer to the the usual freeze-out scenario, as shown by the red curve ($m_Z = 580$ GeV) in Fig. 12 (right).

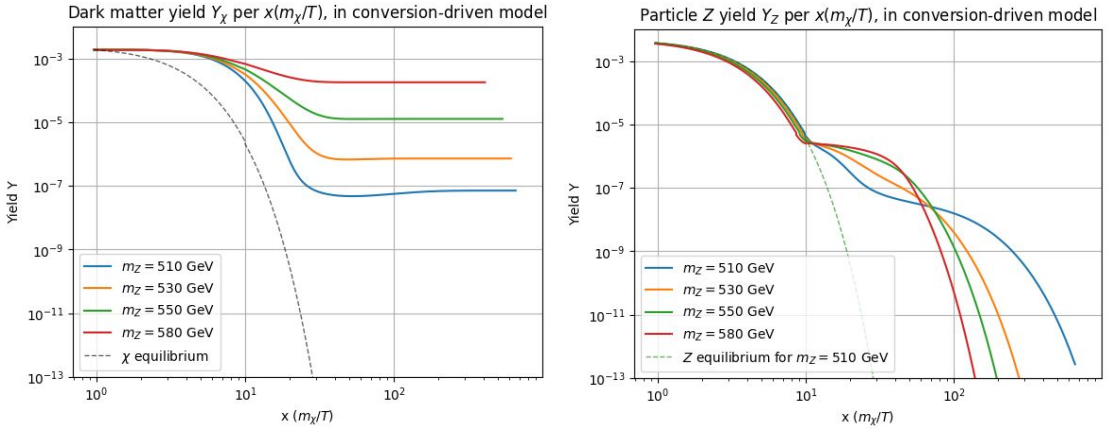


FIG. 12: Dark matter yield $Y_\chi$ (left) and particle $Z$ yield $Y_Z$ (right), along with their equilibrium yields, for the conversion-driven freeze-out model. The model used $m_\chi = 500$ GeV, $\langle\sigma v\rangle_{\chi\chi} = 10^{-40}\text{GeV}^{-2}$, $\Gamma_Z = 10^{-15}$ GeV,$\Gamma_{Z\to\chi} = 10^{-14}$ GeV, $\langle\sigma v\rangle_{ZZ} = 10^{-13}\text{GeV}^{-2}$, $g_\chi = 1$ and $g_Z = 2$.

In Fig. 13, we show a comparison for different values of the conversion cross section. Diminishing the conversion cross section will maintain Dark Matter yield constant for a longer period at early times, because conversions $\chi + SM \to Z + SM$, that dilute Dark Matter, will occur more rarely. Also, the final Dark Matter yield will be larger. On the other hand, if the cross section is large, it can bring the Dark Matter back to thermal equilibrium, as shown by the blue curve in Fig. 13 (left). The $Z$ yield is also strongly affected by the conversion cross section. In particular, for the two smaller values of cross section considered, we see a peak on $Y_Z$ soon after its decoupling temperature ($x \simeq 10$). This is caused by the fact that the majority of $\chi + SM \to Z + SM$ reactions take place when $Z$ is decoupling or has decoupled, so the $Z$ particles created by the conversion process no longer self-annihilate, thus enhancing $Y_Z$. For larger temperatures $Z$ starts to decay, reducing its yield. This reaction produces $\chi$ particles, but it corresponds to a tiny fraction of the total Dark Matter yield and does not cause any visible changes in $Y_\chi$.

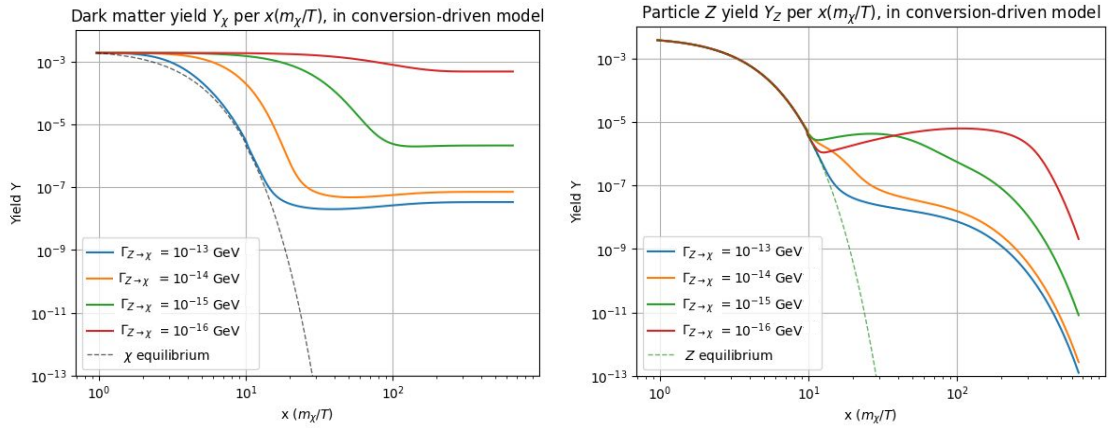


FIG. 13: Dark matter yield $Y_\chi$ (left) and particle $Z$ yield $Y_Z$ (right), along with their equilibrium yields, for the conversion-driven freeze-out model, for different values of $\Gamma_{Z\to\chi}$. The model used $m_\chi = 500$ GeV, $m_Z = 510$ GeV, $\langle\sigma v\rangle_{\chi\chi} = 10^{-40}\text{GeV}^{-2}$, $\Gamma_Z = 10^{-15}$ GeV, $\langle\sigma v\rangle_{ZZ} = 10^{-13}\text{GeV}^{-2}$, $g_\chi = 1$ and $g_Z = 2$.

### 4.4. Freeze-In

A different model for Dark Matter genesis can take place if we consider that Dark Matter may not be in thermal equilibrium at early times. If the DM coupling to the plasma is very small, it will never be in thermal equilibrium, and will react very rarely with the Standard Model particles. Although the DM number density can be close to zero at high temperatures, its yield can be increased due to interactions of other particles. This is called the *freeze-in* mechanism.

For our work, we consider two different reactions that produce DM: the decay of $Z$ ($Z \to \chi + SM$) and conversions ($Z + SM \to \chi + SM$). Dark matter production stops when $Y_Z$ is too low, due to annihilation through reactions or to Boltzmann suppression, and it can no longer produce DM at a relevant rate. At this state, Dark Matter yield becomes constant.

#### 1. *Freeze-in through decays*

Firstly, we shall consider a model where DM production is caused by $Z$ decay. DM self-annihilation rate is very low, as will be shown later. Thus, the main reactions that take place in this mechanism are the decay of $Z$ ($Z \leftrightarrow \chi + SM$), and self-annihilation of $Z$ ($Z + Z \leftrightarrow SM + SM$).

[38, 55–57]. The employment of this model assumes:

$$\begin{gathered}\langle\sigma v\rangle_{\chi Z}=\Gamma_{Z\to\chi}=\langle\sigma v\rangle_{ZZ\to\chi\chi}=0\\ Y_\chi\simeq 0, \text{for } x\ll 1\end{gathered} \tag{105}$$

reducing general Boltzmann Equation to:

$$\frac{dY_\chi}{dx}=\frac{1}{3H}\left|\frac{ds}{dx}\right|\left[-\langle\sigma v\rangle_{\chi\chi}(Y_\chi^2-\overline{Y}_\chi^2)+\frac{K_1(m_Z/T)}{K_2(m_Z/T)}\frac{\Gamma_Z}{s}\left(Y_Z-Y_\chi\frac{\overline{Y}_Z}{\overline{Y}_\chi}\right)\right], \tag{106}$$

$$\frac{dY_Z}{dx}=\frac{1}{3H}\left|\frac{ds}{dx}\right|\left[-\langle\sigma v\rangle_{ZZ}(Y_Z^2-\overline{Y}_Z^2)-\frac{K_1(m_Z/T)}{K_2(m_Z/T)}\frac{\Gamma_Z}{s}\left(Y_Z-Y_\chi\frac{\overline{Y}_Z}{\overline{Y}_\chi}\right)\right]. \tag{107}$$

where $K_n(x)$ are the modified Bessel functions of second kind.

In Fig. 14, we notice that the Feynman diagrams for reactions $Z\leftrightarrow\chi+SM$ and t-channel $\chi+\chi\leftrightarrow SM+SM$ are closely related, as they can be associated by a diagram rotation. However, whereas the decay of the particle $Z$ only has one vertex, Dark Matter self-annihilation has two vertices. For freeze-in, we consider the coupling constant for this vertex $\lambda$ to be very small. Hence, $\chi$ self-annihilation rate will be proportional to $\lambda^2$, and be subdominant. DM self-annihilation will also be subdued due to $Y_\chi$ being very low throughout the whole process.

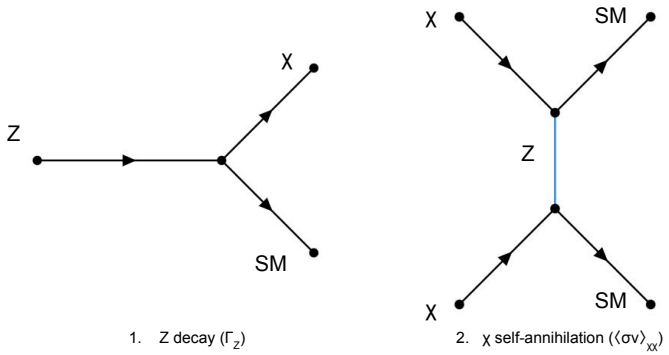


FIG. 14: Feynman diagrams for reactions $Z\leftrightarrow\chi+SM$ (left) and t-channel $\chi+\chi\leftrightarrow SM+SM$ (right).

Setting a model with $m_\chi=500$ GeV, $m_Z=5000$ GeV, $\langle\sigma v\rangle_{\chi\chi}=10^{-35}\text{GeV}^{-2}$, $\Gamma_Z=10^{-21}$ GeV, $\langle\sigma v\rangle_{ZZ}=10^{-5}\text{GeV}^{-2}$, and $g_\chi=g_Z=1$, we obtain the results shown in Fig. 15. At early times, Dark Matter yield is negligible, as is characteristic for the freeze-in mechanism. In this period, $Z$ is relativistic and its yield is kept constant due to reaction $Z+Z\leftrightarrow SM+SM$ occurring efficiently. As the Universe expands, its energy density declines, and the particles in the thermal bath (which, in this case, are $Z$ and the Standard Model particles) lose energy. At $x\simeq 0.1$, the temperature falls under $m_Z$, causing its yield to be Boltzmann suppressed.

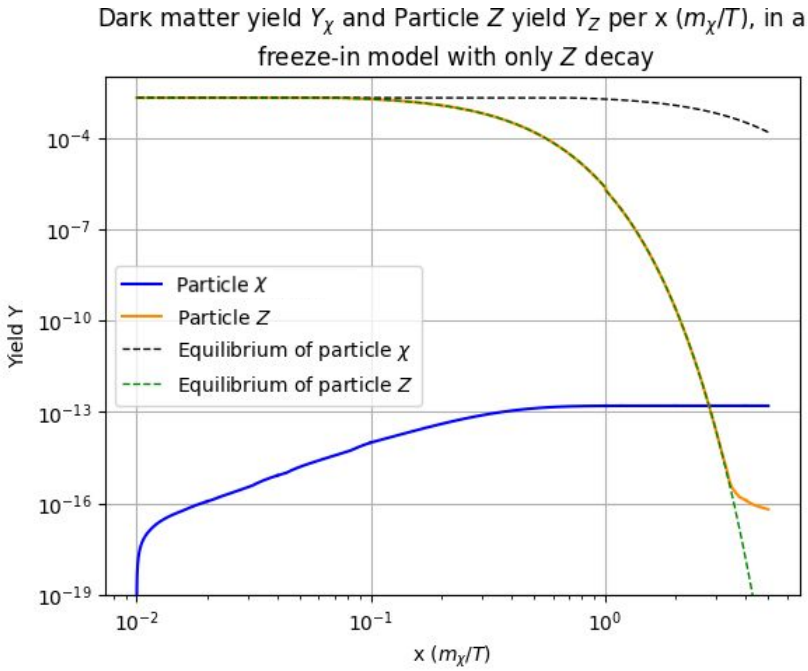


FIG. 15: Dark matter yield (blue) and particle Z yield (orange), along with their equilibrium yields (slashed), in a freeze-in model through $Z$ decays. For the graph, we considered a model with $m_\chi = 500$ GeV, $m_Z = 5000$ GeV, $\langle\sigma v\rangle_{\chi\chi} = 10^{-35}\text{GeV}^{-2}$, $\Gamma_Z = 10^{-21}$ GeV, $\langle\sigma v\rangle_{ZZ} = 10^{-5}\text{GeV}^{-2}$, and $g_\chi = g_Z = 1$.

While $Z$ is in thermal equilibrium, we can rewrite the decay term in Eq. 106 as:

$$\frac{\Gamma_Z}{s}\left(\overline{Y}_Z - Y_\chi\frac{\overline{Y}_Z}{\overline{Y}_\chi}\right) = \frac{\Gamma_Z}{s}\overline{Y}_Z\left(1 - \frac{Y_\chi}{\overline{Y}_\chi}\right) \tag{108}$$

Thus, since $Y_\chi/\overline{Y}_\chi \ll 1$, this term will cause a fraction of $Z$ density to decay through $Z \to \chi + SM$, increasing $Y_\chi$. Nonetheless, this fraction is too small to cause any visible effect in $Y_Z$.

Subsequently, around $x \simeq 0.7$, $Y_Z$ is sufficiently small and its decay no longer contributes significantly to the Dark Matter yield, which reaches a plateau. At this point, $\chi$ has frozen-in, and its yield will remain constant. Particle $Z$ continues to self-annihilate until $x \simeq 3$, when it begins to decouple from the thermal bath. When that occurs, $Z$ yield is too low for its decay to alter DM yield any further.

We can obtain an analytical solution for Eq. 106, in order to obtain an expression for the final yield of Dark Matter. To facilitate our work, we can rewrite Eq. 106 in function of $y$ [55]:

$$y = \frac{m_Z}{T} \tag{109}$$

leading to:

$$\frac{dY_\chi}{dy} = \frac{1}{3H}\left|\frac{ds}{dy}\right|\left[-\langle\sigma v\rangle_{\chi\chi}(Y_\chi^2 - \overline{Y}_\chi^2) + \frac{K_1(y)}{K_2(y)}\frac{\Gamma_Z}{s}\left(Y_Z - Y_\chi\frac{\overline{Y}_Z}{\overline{Y}_\chi}\right)\right] \tag{110}$$

Dark matter self-annihilation is subdominant in this model, thus we can neglect its effect:

$$\frac{dY_\chi}{dy} = \frac{1}{3H}\left|\frac{ds}{dy}\right|\left[\frac{K_1(y)}{K_2(y)}\frac{\Gamma_Z}{s}\left(Y_Z - Y_\chi\frac{\overline{Y}_Z}{\overline{Y}_\chi}\right)\right] \tag{111}$$

During the majority of DM production, $Y_\chi/\bar{Y}_\chi \ll Y_Z/\bar{Y}_Z$, hence:

$$\frac{dY_\chi}{dy} \simeq \frac{1}{3H}\left|\frac{ds}{dy}\right|\left[\frac{K_1(y)}{K_2(y)}\frac{\Gamma_Z}{s}Y_Z\right] \tag{112}$$

and $Z$ is in thermal equilibrium in this interval:

$$\frac{dY_\chi}{dy} = \frac{1}{3H}\left|\frac{ds}{dy}\right|\frac{K_1(y)}{K_2(y)}\frac{\Gamma_Z}{s}\overline{Y}_Z \tag{113}$$

Integrating between $y = 0.1$ and $y = 10$ (i.e. between $x = 0.01$ and $x = 1$), where the majority of DM production occurs:

$$\int_{0.1}^{10}\frac{dY_\chi}{dy}dy = \int_{0.1}^{10}\frac{1}{3H}\left|\frac{ds}{dy}\right|\frac{K_1(y)}{K_2(y)}\frac{\Gamma_Z}{s}\overline{Y}_Z dy \tag{114}$$

Recovering the approximation for $H$ obtained in Eq. 51, the equilibrium yields in Eq. 42 and Eq. 37, and using:

$$\frac{ds}{dy} = \frac{-6\pi^2 g_{*s}}{45}\frac{m_Z^3}{y^4} \tag{115}$$

we rewrite:

$$Y_{10} - Y_{0.1} = \sqrt{\frac{45}{4\pi^3 G g_*}}\frac{\Gamma_Z}{m_z^2}\left[\int_{0.1}^{2/3}\frac{K_1(y)}{K_2(y)}y\frac{135\zeta(3)}{8\pi^4 g_{*s}}dy + \int_{2/3}^{10}y^3 K_1(y)\frac{45}{4\pi^4 g_{*s}}dy\right] \tag{116}$$

$Y_{0.1} \simeq 0$, and, at $y = 10$, DM yield is already constant:

$$Y_{10} = Y_\infty = \frac{3.98\times10^{18}}{\sqrt{g_*}g_{*s}}\frac{\Gamma_Z}{m_Z^2} \tag{117}$$

For the model shown in Fig. 15, we obtain $Y_\infty = 1.59\times10^{-13}$, which show a great concordance with the numerical value $Y = 1.58\times10^{-13}$. This leads to:

$$\Omega_\chi h^2 = \frac{6\times10^{27}m_\chi}{\sqrt{g_*}g_{*s}}\frac{\Gamma_Z}{m_Z^2} \tag{118}$$

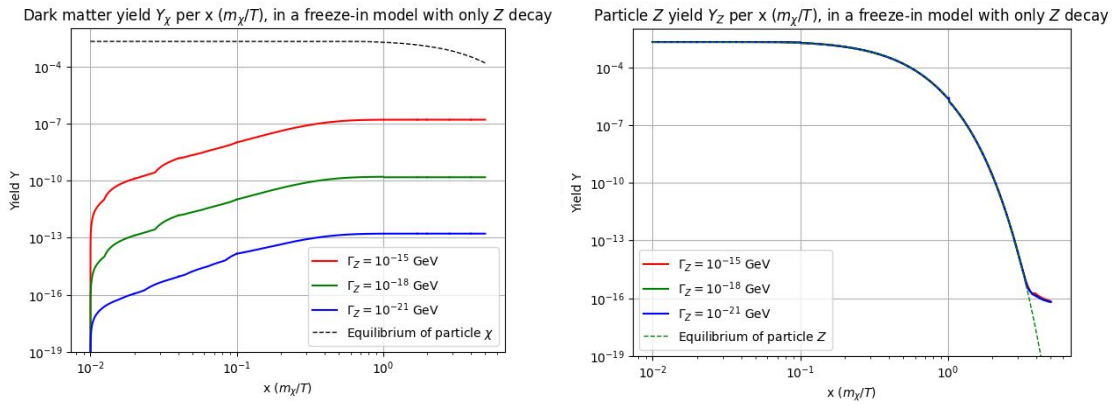


FIG. 16: Dark matter yield (left) and particle $Z$ yield (right), with their equilibrium yields, for different values of $\Gamma_Z$. The model used $m_\chi = 500$ GeV, $m_Z = 5000$ GeV, $\langle\sigma v\rangle_{\chi\chi} = 10^{-35}\text{GeV}^{-2}$, $\langle\sigma v\rangle_{ZZ} = 10^{-5}\text{GeV}^{-2}$, and $g_\chi = g_Z = 1$

Again, as made previously for the other models, we shall analyse how changes in the main model parameters alter the final yield of both particles. In Fig 16, we compare the effect of different values of $\Gamma_Z$. We see that, by increasing the value of $\Gamma_Z$, we expand the $Z \to \chi + SM$ reaction rate, therefore producing more Dark Matter than in the model portrayed in Fig. 15. The decaying particles are still too small of a fraction of the total population of $Z$, and do not cause a significant effect on $Y_Z$ for all cases considered. This relation is in accordance with the analytical expression in Eq. 118, where the final yield of DM is proportional to $\Gamma_Z$.

Lastly, in Fig. 17, we compare this model for different values of $m_Z$. We note that, by increasing the value of $m_Z$, we cause the $m_Z/T$ ratio to be larger than 1 for higher temperatures, therefore accelerating the $Z$ yield Boltzmann suppression. This leads $Y_Z$ to decline sooner, as seen in the right side of Fig. 17. The lower value of $Y_Z$ subsequently to $x \simeq 0.1$ causes a decline in the decay reaction rate, once we have less $Z$ particles available to react as $Z \to \chi + SM$. This impacts the final stages of Dark Matter production, reducing the rate with which DM particles are created. Hence, the larger the value of $m_Z$, the lower the final yield of DM, as seen in Fig. 17 (left). This is expected when we analyse the analytical expression obtained in Eq. 118, where the final yield of DM is inversely proportional to $m_Z$.

### 2. *Freeze-in through* $2 \to 2$ *conversions*

In our second model for the freeze-in mechanism, we consider that the DM production occurs mainly through conversions $Z + SM \to \chi + SM$. [38, 57–59]. The conversion reaction is closely

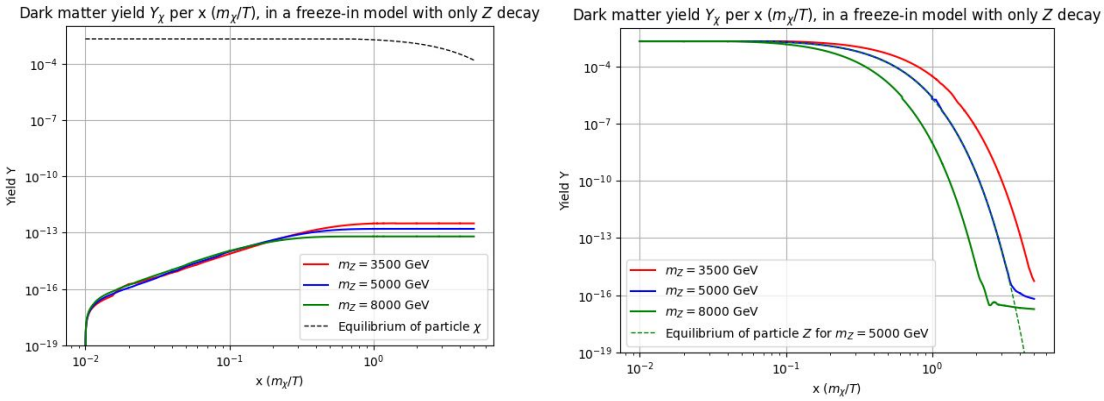


FIG. 17: Dark matter yield (left) and particle $Z$ yield (right), for different values of $m_Z$. The model counted with $m_\chi = 500$ GeV, $\langle\sigma v\rangle_{\chi\chi} = 10^{-35}\text{GeV}^{-2}$, $\Gamma_Z = 10^{-21}$ GeV, $\langle\sigma v\rangle_{ZZ} = 10^{-5}\text{GeV}^{-2}$, and $g_\chi = g_Z = 1$.

related to the three body decay of $Z$ through $Z \leftrightarrow \chi + SM + SM$, and to the co-annihilation reaction $\chi + Z \leftrightarrow SM + SM$, as can be seen in Fig. 4. However, due to the small value of $Y_\chi$ throughout the whole process, the co-annihilation reaction will be subdominant. The application of this mechanism requires:

$$\begin{aligned} \langle\sigma v\rangle_{\chi\chi} = \langle\sigma v\rangle_{\chi\chi\to ZZ} = 0 \\ Y_\chi \simeq 0, \text{for } x \ll 1 \end{aligned} \tag{119}$$

reducing Boltzmann Equation to:

$$\begin{aligned} \frac{dY_\chi}{dx} = \frac{1}{3H}\left|\frac{ds}{dx}\right| \Big[-\langle\sigma v\rangle_{\chi Z}(Y_\chi Y_Z - \overline{Y}_\chi \overline{Y}_Z) \\ + \frac{K_1(m_Z/T)}{K_2(m_Z/T)}\frac{\Gamma_Z}{s}\left(Y_Z - Y_\chi\frac{\overline{Y}_Z}{\overline{Y}_\chi}\right) + \frac{\Gamma_{Z\to\chi}}{s}\left(Y_Z - \overline{Y}_Z\frac{Y_\chi}{\overline{Y}_\chi}\right)\Big], \end{aligned} \tag{120}$$

$$\begin{aligned} \frac{dY_Z}{dx} = \frac{1}{3H}\left|\frac{ds}{dx}\right| \Big[-\langle\sigma v\rangle_{ZZ}(Y_Z^2 - \overline{Y}_Z^2) - \langle\sigma v\rangle_{\chi Z}(Y_\chi Y_Z - \overline{Y}_\chi \overline{Y}_Z) \\ - \frac{K_1(m_Z/T)}{K_2(m_Z/T)}\frac{\Gamma_Z}{s}\left(Y_Z - Y_\chi\frac{\overline{Y}_Z}{\overline{Y}_\chi}\right) - \frac{\Gamma_{Z\to\chi}}{s}\left(Y_Z - \overline{Y}_Z\frac{Y_\chi}{\overline{Y}_\chi}\right)\Big] \end{aligned} \tag{121}$$

Using a model with $m_\chi = 500$ GeV, $m_Z = 5000$ GeV, $\Gamma_{Z\to\chi} = 10^{-22}$ GeV, $\Gamma_Z = 10^{-23}$ GeV, $\langle\sigma v\rangle_{ZZ} = 10^{-5}\text{GeV}^{-2}$, and $g_\chi = g_Z = 1$, we obtain Fig. 18. We see a pattern very similar to a freeze-in through decay model (Fig. 15). At high temperatures, Dark Matter yield is negligible, as assumed for the freeze-in mechanism. $Z$ is relativistic, and its yield is constant due to reaction $Z + Z \leftrightarrow SM + SM$ occurring efficiently. As the Universe expands, its temperature declines,

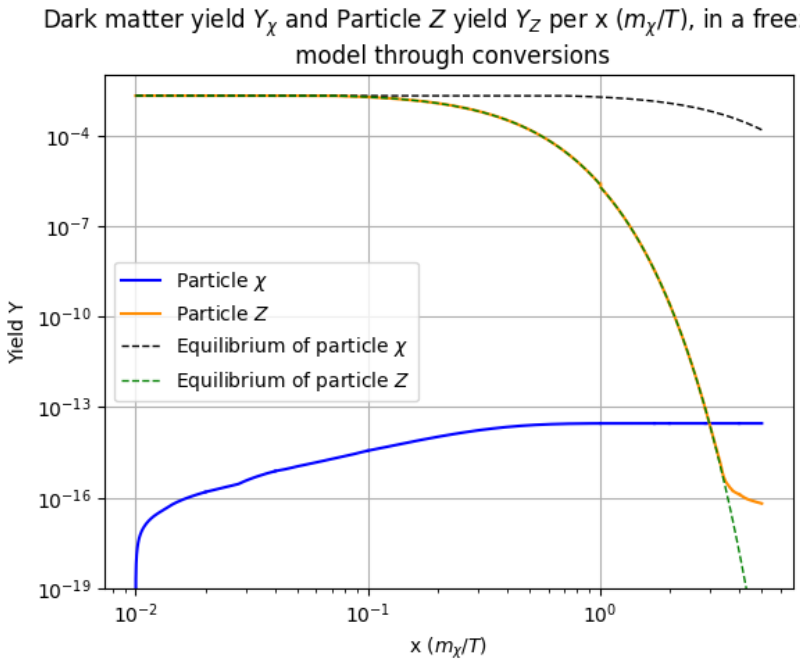


FIG. 18: Dark matter yield (blue) and particle $Z$ yield (orange), in a freeze-in through conversions model. The model used $m_\chi = 500$ GeV, $m_Z = 5000$ GeV, $\Gamma_{Z\to\chi} = 10^{-22}$ GeV, $\Gamma_Z = 10^{-23}$ GeV, $\langle\sigma v\rangle_{ZZ} = 10^{-5}\text{GeV}^{-2}$, and $g_\chi = g_Z = 1$.

causing all particles in the thermal bath (in this case, $Z$ and the Standard Model particles) to lose energy. Thus, subsequently to $x \simeq 0.1$, $Z$ yield becomes Boltzmann suppressed.

While $Z$ is in thermal equilibrium, the conversion term in Eq. 120 can be written as:

$$\frac{\Gamma_{Z\to\chi}}{s}\left(\overline{Y}_Z - Y_\chi\frac{\overline{Y}_Z}{\overline{Y}_\chi}\right) = \frac{\Gamma_{Z\to\chi}}{s}\overline{Y}_Z\left(1 - \frac{Y_\chi}{\overline{Y}_\chi}\right) \tag{122}$$

And the decay term can be rewritten as:

$$\frac{\Gamma_Z}{s}\left(\overline{Y}_Z - Y_\chi\frac{\overline{Y}_Z}{\overline{Y}_\chi}\right) = \frac{\Gamma_Z}{s}\overline{Y}_Z\left(1 - \frac{Y_\chi}{\overline{Y}_\chi}\right) \tag{123}$$

At early times, $Y_\chi \simeq 0$, which will enhance $Z + SM \to \chi + SM$ conversions, and cause a fraction of $Z$ to decay through $Z \to \chi + SM + SM$. Both these processes will increase $Y_\chi$, as seen in Fig. 18.

As $Z$ yield starts to become Boltzmann suppressed, the conversion rate begins to decrease. At $x \simeq 0.7$, the conversion rate is much smaller than for $x < 0.1$, and Dark Matter yield is large enough to not feel the effect of $Z$ decay. Subsequently to this point, $Y_\chi$ is constant, and Dark

Matter has frozen in. $Z$ continues to self-annihilate until $x \simeq 4$, when decouples from the thermal bath.

For an analytical solution of Dark Matter final yield, it is favorable to rewrite Eq. 120 in function of $y = m_Z/T$ [58]:

$$\frac{dY_\chi}{dy} = \frac{1}{3H}\left|\frac{ds}{dy}\right|\left[-\langle\sigma v\rangle_{\chi Z}(Y_\chi Y_Z - \overline{Y}_\chi \overline{Y}_Z) + \frac{K_1(y)}{K_2(y)}\frac{\Gamma_Z}{s}\left(Y_Z - Y_\chi\frac{\overline{Y}_Z}{\overline{Y}_\chi}\right) + \frac{\Gamma_{Z\to\chi}}{s}\left(Y_Z - \overline{Y}_Z\frac{Y_\chi}{\overline{Y}_\chi}\right)\right] \tag{124}$$

We can approach $Y_\chi \simeq 0$ for the whole process:

$$\frac{dY_\chi}{dy} = \frac{1}{3H}\left|\frac{ds}{dy}\right|\left[\frac{K_1(y)}{K_2(y)}\frac{\Gamma_Z}{s}Y_Z + \frac{\Gamma_{Z\to\chi}}{s}Y_Z\right] \tag{125}$$

$Z$ is in thermal equilibrium during the production of $\chi$:

$$\frac{dY_\chi}{dy} = \frac{1}{3H}\left|\frac{ds}{dy}\right|\left[\frac{K_1(y)}{K_2(y)}\frac{\Gamma_Z}{s}\overline{Y}_Z + \frac{\Gamma_{Z\to\chi}}{s}\overline{Y}_Z\right] \tag{126}$$

For the decay term, we can recover the analytical expression obtained for the freeze-in through decays model, along with the approximations for $H$ and $ds/dy$ (Eq. 51 and Eq. 115):

$$Y_\infty = Y_\infty^{decay} + \sqrt{\frac{45}{4\pi^3 G g_*}}\frac{1}{m_Z^2}\int_{0.1}^{10} y\Gamma_{Z\to\chi}\overline{Y}_Z dy \tag{127}$$

$$Y_\infty = Y_\infty^{decay} + \sqrt{\frac{45}{4\pi^3 G g_*}}\frac{\Gamma_{Z\to\chi}}{m_Z^2}\left[\int_{0.1}^{2/3} y\frac{135\zeta(3)}{8\pi^4 g_{*s}}dy + \int_{2/3}^{10} y^3 K_2(y)\frac{45}{4\pi^4 g_{*s}}dy\right] \tag{128}$$

Leading to:

$$Y_\infty = \frac{1}{\sqrt{g_*}g_{*s}}\frac{1}{m_Z^2}(3.98\times 10^{18}\Gamma_Z + 6.757\times 10^{18}\Gamma_{Z\to\chi}) \tag{129}$$

For the model used in Fig. 18, we obtain $Y_\infty = 2.86\times 10^{-14}$, which is in great agreement with the numerical value $2.88\times 10^{-14}$. Dark matter abundance becomes:

$$\Omega h^2 = \frac{m_\chi}{\sqrt{g_*}g_{*s}}\frac{1}{m_Z^2}(6\times 10^{27}\Gamma_Z + 4.0869\times 10^{27}\Gamma_{Z\to\chi}) \tag{130}$$

As made previously for the other mechanisms, we shall compare how changes in the main parameters of the model ($\Gamma_{Z\to\chi}$ and $m_Z$) impact the behaviour of both particles.

In Fig. 19, we remark that, the higher the value of $\Gamma_{Z\to\chi}$, the larger will the conversion $Z + SM \to \chi + SM$ rate be, thus producing more Dark Matter. The assumption that $\Gamma_Z$ is always 10% of $\Gamma_{Z\to\chi}$ also implies that, as $\Gamma_{Z\to\chi}$ increases, so will $\Gamma_Z$. A larger value of $\Gamma_Z$ will increase the fraction of $Z$ decaying, also generating more Dark Matter. These factors, combined, increase the final yield of $\chi$, as seen in Fig. 19 (left). However, for all cases considered, the $Z$ self-annihilation rate is too strong for the majority of the process, therefore $Y_Z$ does not suffer significantly the alterations of conversion and decay rates, as seen in Fig. 19 (right).

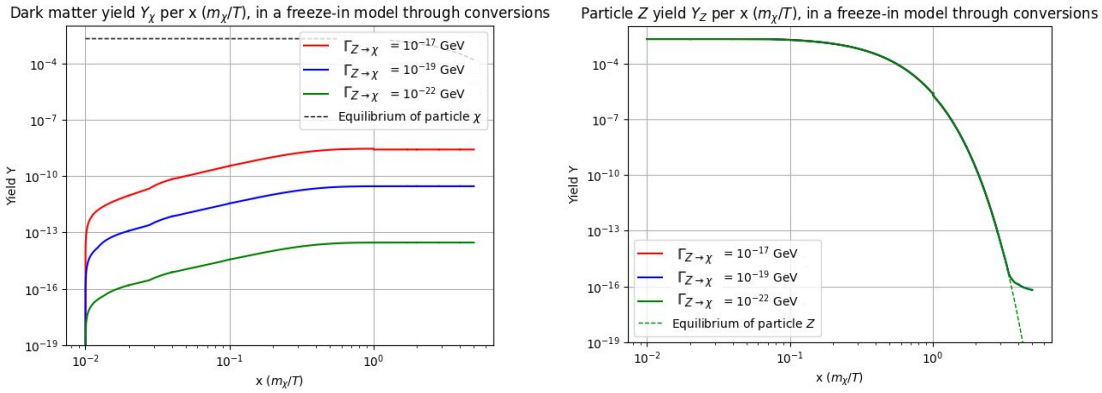


FIG. 19: Dark matter yield (left) and particle $Z$ yield (right), for different values of $\Gamma_{Z\to\chi}$, in a freeze-in through conversions model. The model used $m_\chi = 500$ GeV, $m_Z = 5000$ GeV, $\langle\sigma v\rangle_{ZZ} = 10^{-5}\text{GeV}^{-2}$, $\Gamma_Z = 10\%\Gamma_{Z\to\chi}$, and $g_\chi = g_Z = 1$.

In Fig. 20 (right), we note that a larger value of $m_Z$ will accelerate its Boltzmann suppression, once the $m_Z/T$ ratio will become larger than 1 for higher temperatures. This causes the $Z$ yield to decline sooner. A reduced the value of $Y_Z$ will lead to a decline in the production of Dark Matter (i.e. the conversion rate will be suppressed), once we have less $Z$ particles to react as $Z + SM \to \chi + SM$. This is noticeable in the left side of Fig. 20, where the Dark Matter yield is lower for larger values of $m_Z$ subsequently to $x \simeq 0.1$.

## 5. CONCLUSIONS

In this work, different possible mechanisms for Dark Matter genesis were addressed and analysed. Using a computational program, it was possible to integrate the Boltzmann Equation for both Dark Matter and $Z$, a generic particle beyond the Standard Model. This integration ensue

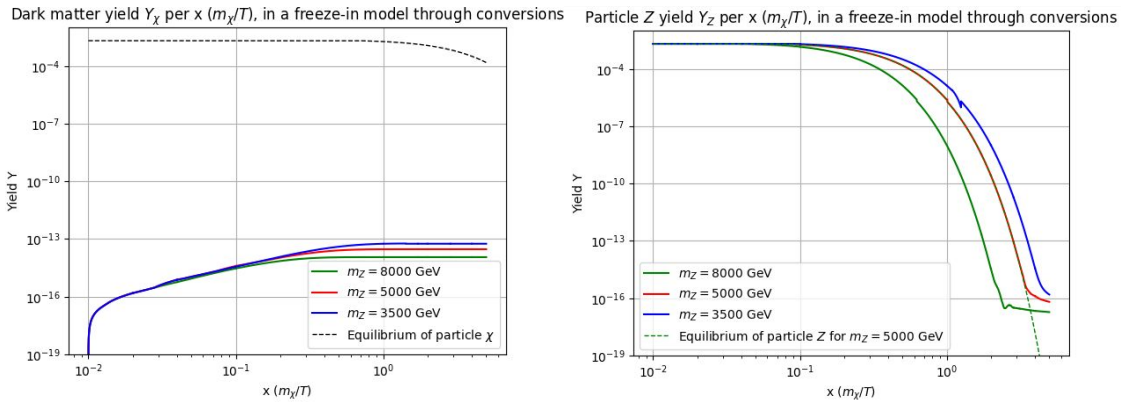


FIG. 20: Dark matter yield (left) and particle $Z$ yield (right), for different values of $m_Z$, in a freeze-in through conversions model. The model used $m_\chi = 500$ GeV, $\Gamma_{Z\to\chi} = 10^{-22}$ GeV, $\Gamma_Z = 10^{-23}$ GeV, $\langle\sigma v\rangle_{ZZ} = 10^{-5}\text{GeV}^{-2}$, and $g_\chi = g_Z = 1$..

the yield of both particles at all temperatures of interest. These results specify both particles behaviour as temperature drops, allowing us a better understanding of how these models work, and how they are affected by changes in particles' mass and interaction cross section. It also propitiate a deeper comprehension about how each model and their main parameters impact the Dark Matter abundance, and which one of them can proportionate the actual DM abundance seen in our Universe, $\Omega h^2 = 0.12$.

The software developed for this work is able to simulate intermediary models, which allow for construction of new mechanisms in addition to the ones considered here.

It also opens windows for improvement of the code, such as considering multi-component Dark Matter, using Quantum Field Theory for calculating the cross sections for each reaction.

## Appendix A: Derivation of the Boltzmann Equation for DM

The evolution of a particle $i$'s number distribution is described through Boltzmann Equation [31]:

$$\frac{\partial F_i(p,t)}{\partial t} - Hp\frac{\partial F_i(p,t)}{\partial p} = C_i(F_i, F_j, p) \tag{A1}$$

where we have assumed Universe isotropy. $F_i(p,t)$ is the number distribution for particle $i$ with momentum $p$, $H$ is the Hubble constant, and $C$ is a collision term that represents all the interactions that particle $i$ suffers. This term depends on the number distribution of particle $j$, that interacts with particle $i$. With $F_i(p,t)$, we can write:

$$n_i(t) = \int F_i(p,t)p^2\frac{dp}{2\pi^2} \tag{A2}$$

where $n_i(t)$ represents particle $i$'s number density, that changes with time. Using this expression, we can rewrite Boltzmann Equation as:

$$\frac{dn_i}{dt} + 3Hn_i = \int C_i p^2\frac{dp}{2\pi^2} \tag{A3}$$

The collision term for particle $i$ is given by:

$$C_i = C_{annihilation} + C_{production} + C_{decay} \tag{A4}$$

where the contributions for this expression come from the different processes particle $i$ can participate in. We must derive each of these expressions separately. We begin by considering an annihilation between 4 particles $i, j, a, b$, none of which we consider initially to be in thermal equilibrium. Taking form as $i + j \leftrightarrow a + b$, the collision term for this reaction is given by:

$$\begin{aligned}\int C_{ann}p^2\frac{dp}{2\pi^2} = \int \frac{d^3p_i}{2E_i(2\pi)^3}\frac{d^3p_j}{2E_j(2\pi)^3}\frac{d^3p_a}{2E_a(2\pi)^3}\frac{d^3p_b}{2E_b(2\pi)^3}(2\pi)^4\delta^4(p_i + p_j - p_a - p_b) \\ |\mathcal{M}|^2[(1 \pm f_a)(1 \pm f_b)f_i f_j - f_a f_b(1 \pm f_i)(1 \pm f_j)]\end{aligned} \tag{A5}$$

where $\mathcal{M}$ represents the amplitude matrix, and the $\delta$ term enforces momentum conservation. The $+$ signs are for bosons, and the $-$ signs are for fermions. Assuming that $f_a, f_b, f_i, f_j \ll 1$:

$$\int C_{ann}p^2\frac{dp}{2\pi^2} = \int \frac{d^3p_i}{2E_i(2\pi)^3}\frac{d^3p_j}{2E_j(2\pi)^3}\frac{d^3p_a}{2E_a(2\pi)^3}\frac{d^3p_b}{2E_b(2\pi)^3}(2\pi)^4\delta^4(p_i+p_j-p_a-p_b)|M|^2[f_i f_j - f_a f_b] \tag{A6}$$

Using Fermi-Dirac or Bose-Einstein statistics, it is possible to rewrite the distributions as:

$$f_i = \frac{1}{\exp((E_i - \mu_i)/k_B T) \pm 1} \tag{A7}$$

where + stands for fermions and − stands for bosons, $k_B$ is the Boltzmann constant, and $\mu_i$ is particle $i$'s chemical potential. Taking natural units for all the quantities used in our work, $k_B = 1$. Previously, we assumed that $f_a, f_b, f_i, f_j \ll 1$, hence the $\pm 1$ term will have negligible influence. With this, we rewrite the distribution functions as:

$$f_i = \exp(-(E_i - \mu_i)/T) \tag{A8}$$

$$\Rightarrow \int C_{ann} p^2 \frac{dp}{2\pi^2} = \int \frac{d^3p_i}{2E_i(2\pi)^3} \frac{d^3p_j}{2E_j(2\pi)^3} \frac{d^3p_a}{2E_a(2\pi)^3} \frac{d^3p_b}{2E_b(2\pi)^3} (2\pi)^4 \delta^4(p_i + p_j - p_a - p_b) |M|^2 \\ [\exp(-(E_i - \mu_i + E_j - \mu_j)/T) - \exp(-(E_a - \mu_a + E_b - \mu_b)/T)] \tag{A9}$$

hence, using conservation of energy $E_i + E_j = E_a + E_b$,:

$$\exp(-(E_i + E_j)/T) = \exp(-(E_a + E_b)/T) \tag{A10}$$

we can use $\exp(-(E_i + E_j)/T)$ as a common multiplier:

$$\int C_{ann} p^2 \frac{dp}{2\pi^2} = -\int \frac{d^3p_i}{2E_i(2\pi)^3} \frac{d^3p_j}{2E_j(2\pi)^3} \frac{d^3p_a}{2E_a(2\pi)^3} \frac{d^3p_b}{2E_b(2\pi)^3} (2\pi)^4 \delta^4(p_i + p_j - p_a - p_b) |M|^2 \\ \exp(-(E_i + E_j)/T)[\exp((\mu_i + \mu_j)/T) - \exp((\mu_a + \mu_b)/T)] \tag{A11}$$

Assuming that, for all cases of interest, chemical potential $\mu$ is zero for all particles involved in the process, we can use Maxwell-Boltzmann similarity approximation, that states [60]:

$$f_i = \frac{n_i}{\overline{n}_i} \overline{f}_i \tag{A12}$$

for cases when particle $i$ is in kinetic equilibrium with the thermal bath. Hence, using:

$$\frac{f_i}{\overline{f}_i} = \exp(\mu_i/T) \tag{A13}$$

$$\rightarrow \exp(\mu_i/T) = \frac{n_i}{\overline{n}_i} \tag{A14}$$

which implies:

$$\Rightarrow \int C_{ann} p^2 \frac{dp}{2\pi^2} = -\int \frac{d^3p_i}{2E_i(2\pi)^3} \frac{d^3p_j}{2E_j(2\pi)^3} \frac{d^3p_a}{2E_a(2\pi)^3} \frac{d^3p_b}{2E_b(2\pi)^3} (2\pi)^4 \delta^4(p_i + p_j - p_a - p_b) |M|^2 \\ [\exp(-(E_i + E_j)/T)] \left[ \frac{n_i n_j}{\overline{n}_i \overline{n}_j} - \frac{n_a n_b}{\overline{n}_a \overline{n}_b} \right] \tag{A15}$$

therefore:

$$\int C_{ann} p^2 \frac{dp}{2\pi^2} = -\langle \sigma v \rangle \left( \frac{n_i n_j}{\overline{n}_i \overline{n}_j} - \frac{n_a n_b}{\overline{n}_a \overline{n}_b} \right) \tag{A16}$$

For the special case of self-annihilation $i+i \leftrightarrow a+b$, where $a$ and $b$ are in thermal equilibrium, we obtain:

$$\int C_{ann} p^2 \frac{dp}{2\pi^2} = -\langle \sigma v \rangle \left( \frac{n_i^2}{\overline{n}_i^2} - 1 \right) = -\langle \sigma v \rangle (n_i^2 - \overline{n}_i^2) \tag{A17}$$

For the decay term, we consider a reaction $i \leftrightarrow a+b$, and that $BR(i \to a+b) = 1$ (i.e., particle $i$ always decays in $a$ and $b$). This yields:

$$C_{dec} = \frac{1}{E_i} \int \frac{d^3 p_a}{2E_a (2\pi)^3} \frac{d^3 p_b}{2E_b (2\pi)^3} (2\pi)^4 \delta(p_i - p_a - p_b) |\mathcal{M}|^2 [f_i - f_a f_b] \tag{A18}$$

Applying the same approximations used previously:

$$C_{dec} = \left( f_i - \frac{n_a n_b}{\overline{n}_a \overline{n}_b} \overline{f}_i \right) \frac{1}{E_i} \int \frac{d^3 p_a}{2E_a (2\pi)^3} \frac{d^3 p_b}{2E_b (2\pi)^3} (2\pi)^4 \delta(p_i - p_a - p_b) |\mathcal{M}|^2 \tag{A19}$$

$$C_{dec} = BR(i \to a+b) \frac{\Gamma_i m_i}{E_i} \left( f_i - \frac{n_a n_b}{\overline{n}_a \overline{n}_b} \overline{f}_i \right) \tag{A20}$$

where $\Gamma_i$ represents particle $i$'s decay width. Therefore:

$$\int C_{dec} p^2 \frac{dp}{2\pi^2} = -\int \frac{dp}{2\pi^2} p^2 \frac{\Gamma_i m_i}{E_i} f_i + \sum_{i-decays} BR(i \to a+b) \int \frac{\Gamma_i m_i}{E_i} \frac{dp}{2\pi^2} p^2 \frac{n_a n_b}{\overline{n}_a \overline{n}_b} \overline{f}_i \tag{A21}$$

Assuming that:

$$\frac{1}{n_i} \int \frac{1}{E_i} f_i p^2 \frac{dp}{2\pi^2} = \frac{1}{\overline{n}_i} \int \frac{1}{E_i} \overline{f}_i p^2 \frac{dp}{2\pi^2} = \langle \frac{1}{E} \rangle \tag{A22}$$

we can integrate and find [61]:

$$m_i \langle \frac{1}{E} \rangle = \langle \frac{m_i}{E} \rangle = \frac{K_1(m_i/T)}{K_2(m_i/T)} \tag{A23}$$

where $K_n$ are the modified Bessel functions of second kind of order $n$. Hence:

$$\int C_{dec} p^2 \frac{dp}{2\pi^2} = -\frac{K_1(m_i/T)}{K_2(m_i/T)} \Gamma_i \left( n_i - \overline{n}_i \sum_{i-decays} BR(i \to a+b) \frac{n_a n_b}{\overline{n}_a \overline{n}_b} \right) \tag{A24}$$

Lastly, we search for an expression for the production of particle $i$. Considering an interaction $j \leftrightarrow i+b$, we initially have:

$$C_{prod} = \frac{1}{E_i} \int \frac{d^3 p_j}{2E_j (2\pi)^3} \frac{d^3 p_b}{2E_b (2\pi)^3} (2\pi)^4 \delta(p_j - p_i - p_b) |\mathcal{M}|^2 [f_j - f_i f_b] \tag{A25}$$

Therefore, applying the same approximations used previously:

$$C_{prod} = \frac{1}{E_i} \int \frac{d^3 p_j}{2E_j (2\pi)^3} \frac{d^3 p_b}{2E_b (2\pi)^3} (2\pi)^4 \delta(p_j - p_i - p_b) |\mathcal{M}|^2 \left[ f_j - \overline{f}_j \frac{n_i n_b}{\overline{n}_i \overline{n}_b} \right] \tag{A26}$$

which implies:

$$\int C_{prod} p^2 \frac{dp}{2\pi^2} = \int \frac{d^3p_j}{E_j(2\pi)^3} \frac{d^3p}{2E_i(2\pi)^3} \frac{d^3p_b}{2E_b(2\pi)^3} (2\pi)^4 \delta(p_j - p_i - p_b) |\mathcal{M}|^2 \left[ f_j - \overline{f}_j \frac{n_i n_b}{\overline{n}_i \overline{n}_b} \right] \tag{A27}$$

Using again Eq. A23, we obtain:

$$\int C_{prod} p^2 \frac{dp}{2\pi^2} = \frac{K_1(m_j/T)}{K_2(m_j/T)} \Gamma_j \sum BR(j \to \dots) \left( n_j - \overline{n}_j \sum \frac{BR(j \to i+b)}{BR(j \to \dots)} \frac{n_i n_b}{\overline{n}_i \overline{n}_b} \right) \tag{A28}$$

Therefore, we have found all expressions for the collision term, and can now write Boltzmann Equation for Dark Matter, taking into account all processes it may participate:

$$\begin{aligned} \frac{dn_i}{dt} + 3Hn_i = &-\langle \sigma v \rangle (n_i^2 - \overline{n}_i^2) - \frac{K_1(m_i/T)}{K_2(m_i/T)} \Gamma_i \left( n_i - \overline{n}_i \sum_{i-decays} BR(i \to \dots) \frac{n_a n_b}{\overline{n}_a \overline{n}_b} \right) \\ &+ \frac{K_1(m_j/T)}{K_2(m_j/T)} \Gamma_j \sum BR(j \to \dots) \left( n_j - \overline{n}_j \sum \frac{BR(j \to i+b)}{BR(j \to \dots)} \frac{n_i n_b}{\overline{n}_i \overline{n}_b} \right) \end{aligned} \tag{A29}$$

For our analysis, it is convenient to define to new variables:

$$x = \frac{m_\chi}{T} \tag{A30}$$

$$Y_i = \frac{n_i}{s} \tag{A31}$$

where $s$ represents entropy density, and $m_\chi$ is Dark Matter particle's mass. Quantity $Y_i$ is the yield of particle $i$. Entropy density decays by a factor $a^3$, due to Universe expansion. By dividing $n_i$ by entropy density, we cancel this factor, hence the yield will not be altered by the change in Universe volume. Therefore:

$$\frac{dY_i}{dt} = \frac{d}{dt} \left( \frac{n_i}{s} \right) = \frac{dn_i}{dt} \frac{1}{s} - \frac{n_i}{s^2} \frac{ds}{dt} \tag{A32}$$

knowing that, due to the adiabatic expansion of Universe, entropy density must vary as:

$$\frac{ds}{dt} = -3Hs \tag{A33}$$

which implies:

$$\frac{dY_i}{dt} = \frac{dn_i}{dt} \frac{1}{s} + \frac{3Hn_i}{s} \tag{A34}$$

Therefore, using Eq. A29, we get that:

$$\begin{aligned} \frac{dY_i}{dt} = \frac{1}{s} \Bigg[ &-\langle \sigma v \rangle (n_i^2 - \overline{n}_i^2) - \frac{K_1(m_i/T)}{K_2(m_i/T)} \Gamma_i \left( n_i - \overline{n}_i \sum_{i-decays} BR(i \to \dots) \frac{n_a n_b}{\overline{n}_a \overline{n}_b} \right) \\ &+ \frac{K_1(m_j/T)}{K_2(m_j/T)} \Gamma_j \sum BR(j \to \dots) \left( n_j - \overline{n}_j \sum \frac{BR(j \to i+b)}{BR(j \to \dots)} \frac{n_i n_b}{\overline{n}_i \overline{n}_b} \right) - 3Hn_i \Bigg] + \frac{3Hn_i}{s} \end{aligned} \tag{A35}$$

the last two terms cancel each other out, consequently:

$$\frac{dY_i}{dt} = \frac{1}{s}\left[-\langle\sigma v\rangle(n_i^2 - \overline{n}_i^2) - \frac{K_1(m_i/T)}{K_2(m_i/T)}\Gamma_i\left(n_i - \overline{n}_i\sum_{i-decays} BR(i \to \dots)\frac{n_a n_b}{\overline{n}_a\overline{n}_b}\right)\right. \\ \left. + \frac{K_1(m_j/T)}{K_2(m_j/T)}\Gamma_j\sum BR(j \to \dots)\left(n_j - \overline{n}_j\sum\frac{BR(j \to i+b)}{BR(j \to \dots)}\frac{n_i n_b}{\overline{n}_i\overline{n}_b}\right)\right] \tag{A36}$$

However, we wish to write this equation with a dependency of $x$, in order to see how Dark Matter number density changes with temperature, instead of time. To do this, we apply:

$$\left[\frac{dx}{dY_i}\right]^{-1} = \left[\frac{d(m_\chi/T)}{dY_i}\right]^{-1} = \left[\frac{dm_\chi}{dY_i}\frac{1}{T} - \frac{dT}{dY_i}\frac{m_\chi}{T^2}\right]^{-1} \tag{A37}$$

Dark Matter particle mass is constant, hence $dm_\chi/dY_i = 0$.

$$\frac{dY_i}{dx} = -\frac{dY_i}{dT}\frac{T^2}{m_\chi} \tag{A38}$$

which can be rewritten as:

$$\frac{dY_i}{dx} = -\frac{dY_i}{dt}\frac{dt}{dT}\frac{T^2}{m_\chi} \tag{A39}$$

Next, rewriting:

$$\frac{dt}{dT} = \frac{dt}{ds}\frac{ds}{dT} = \frac{-1}{3Hs}\frac{ds}{dT} \tag{A40}$$

and:

$$T = \frac{m_\chi}{x} \tag{A41}$$

where $m_\chi$ is Dark Matter particle's mass. This implies that:

$$\frac{dY_i}{dx} = \frac{1}{3Hs}\frac{m_\chi}{x^2}\frac{ds}{dT}\frac{1}{s}\left[-\langle\sigma v\rangle(n_i^2 - \overline{n}_i^2) - \frac{K_1(m_i/T)}{K_2(m_i/T)}\Gamma_i\left(n_i - \overline{n}_i\sum_{i-decays} BR(i \to \dots)\frac{n_a n_b}{\overline{n}_a\overline{n}_b}\right)\right. \\ \left. + \frac{K_1(m_j/T)}{K_2(m_j/T)}\Gamma_j\sum BR(j \to \dots)\left(n_j - \overline{n}_j\sum\frac{BR(j \to i+b)}{BR(j \to \dots)}\frac{n_i n_b}{\overline{n}_i\overline{n}_b}\right)\right] \tag{A42}$$

and, transforming $n_i = Y_i s$ and $\overline{n}_i = \overline{Y}_i s$:

$$\frac{dY_i}{dx} = \frac{1}{3H}\frac{m_\chi}{x^2}\frac{ds}{dT}\left[-\langle\sigma v\rangle(Y_i^2 - \overline{Y}_i^2) - \frac{K_1(m_i/T)}{K_2(m_i/T)}\frac{\Gamma_i}{s}\left(Y_i - \overline{Y}_i\sum_{i-decays} BR(i \to \dots)\frac{Y_a Y_b}{\overline{Y}_a\overline{Y}_b}\right)\right. \\ \left. + \frac{K_1(m_j/T)}{K_2(m_j/T)}\frac{\Gamma_j}{s}\sum BR(j \to \dots)\left(Y_j - \overline{Y}_j\sum\frac{BR(j \to i+b\, Y_i Y_b)}{BR(j \to \dots)}\frac{}{\overline{Y}_i\overline{Y}_b}\right)\right] \tag{A43}$$

For the expression of $ds/dT$, we can write that, during radiation era (where the majority of candidates of Dark Matter were supposedly created), entropy density was given by:

$$s = \frac{2\pi^2}{45} g_{*s} T^3 \tag{A44}$$

where $g_{*s}$ is the number of effective relativistic degrees of freedom associated with entropy, that can be approximated as $g_{*s} \simeq g_*$, allowing us to use the approximation in Eq. 50. Applying this:

$$\frac{ds}{dT} = \frac{6\pi^2}{45} g_{*s} T^2 \tag{A45}$$

$$\frac{ds}{dx} = \frac{ds}{dT}\frac{dT}{dx} = \frac{ds}{dT}\frac{-m_\chi}{x^2} \tag{A46}$$

therefore we can rewrite:

$$\begin{aligned}\frac{dY_i}{dx} = \frac{-1}{3H}\frac{ds}{dx}\Bigg[-\langle\sigma v\rangle(Y_i^2 - \overline{Y}_i^2) - \frac{K_1(m_i/T)}{K_2(m_i/T)}\frac{\Gamma_i}{s}\left(Y_i - \overline{Y}_i \sum_{i-decays} BR(i \to \dots)\frac{Y_a Y_b}{\overline{Y}_a \overline{Y}_b}\right) \\ + \frac{K_1(m_j/T)}{K_2(m_j/T)}\frac{\Gamma_j}{s}\sum BR(j \to \dots)\left(Y_j - \overline{Y}_j \sum \frac{BR(j \to i+b)}{BR(j \to \dots)}\frac{Y_i Y_b}{\overline{Y}_i \overline{Y}_b}\right)\Bigg]\end{aligned} \tag{A47}$$

For the case of a reaction $a + b \to c + d$, where $b$ and $d$ are in thermal equilibrium, we write:

$$\langle\sigma v\rangle_{a\to c}\left(\frac{Y_a}{\overline{Y}_a} - \frac{Y_c}{\overline{Y}_c}\right) = \frac{\Gamma_{a\to c}}{s}\overline{Y}_a\left(\frac{Y_a}{\overline{Y}_a} - \frac{Y_c}{\overline{Y}_c}\right) = \frac{\Gamma_{a\to c}}{s}\left(Y_a - \overline{Y}_a\frac{Y_c}{\overline{Y}_c}\right) \tag{A48}$$

Consequently, we can arrange these equations to solve for all possible interactions of Dark Matter particle $\chi$ with a particle $Z$ beyond the Standard Model:

$$\begin{aligned}\frac{dY_\chi}{dx} = \frac{1}{3H}\left|\frac{ds}{dx}\right|\Bigg[-\langle\sigma v\rangle_{\chi\chi}(Y_\chi^2 - \overline{Y}_\chi^2) - \langle\sigma v\rangle_{\chi Z}(Y_\chi Y_Z - \overline{Y}_\chi \overline{Y}_Z) + \frac{K_1(m_Z/T)}{K_2(m_Z/T)}\frac{\Gamma_Z}{s}\left(Y_Z - Y_\chi\frac{\overline{Y}_Z}{\overline{Y}_\chi}\right) \\ + \frac{\Gamma_{Z\to\chi}}{s}\left(Y_Z - \overline{Y}_Z\frac{Y_\chi}{\overline{Y}_\chi}\right) + \langle\sigma v\rangle_{ZZ\to\chi\chi}\left(\frac{Y_Z^2}{\overline{Y}_Z^2} - \frac{Y_\chi^2}{\overline{Y}_\chi^2}\right)\Bigg]\end{aligned} \tag{A49}$$

The first term accounts for self-destruction of Dark Matter, in $\chi + \chi \leftrightarrow SM + SM$; the second term represents co-annihilation between $\chi$ and $Z$, in $\chi + Z \leftrightarrow SM + SM$; the third expression constitute for the decay of $Z$ in $\chi$, as in $Z \leftrightarrow \chi + SM$; the fourth term act for collisions between $Z$ with particles from the Standard Model, generating $\chi$, as in $Z + SM \leftrightarrow \chi + SM$; lastly, the fifth expression amount to the double collision of $Z$, for $Z + Z \leftrightarrow \chi + \chi$.

In Eq. 64, the yield of particle $Z$ is used consistently. Hence, we need to write an equation that represents the variation of $Y_Z$, to be able to solve this equation. Using the expressions obtained before, we arrive at:

$$\frac{dY_Z}{dx} = \frac{1}{3H}\left|\frac{ds}{dx}\right|\left[-\langle\sigma v\rangle_{ZZ}(Y_Z^2 - \overline{Y}_Z^2) - \langle\sigma v\rangle_{\chi Z}(Y_\chi Y_Z - \overline{Y}_\chi \overline{Y}_Z) - \frac{K_1(m_Z/T)}{K_2(m_Z/T)}\frac{\Gamma_Z}{s}\left(Y_Z - Y_\chi\frac{\overline{Y}_Z}{\overline{Y}_\chi}\right)\right.$$
$$\left. -\frac{\Gamma_{Z\to\chi}}{s}\left(Y_Z - \overline{Y}_Z\frac{Y_\chi}{\overline{Y}_\chi}\right) - \langle\sigma v\rangle_{ZZ\to\chi\chi}\left(\frac{Y_Z^2}{\overline{Y}_Z^2} - \frac{Y_\chi^2}{\overline{Y}_\chi^2}\right)\right] \tag{A50}$$

where the physical significance of each term is the same as explained for Eq. 64; except for the first term, that in this case accounts for the self-annihilation of $Z$.

---


[1] N. A. et al., Astronomy & Astrophysics **641**, A6 (2020).

[2] J. H. Oort, Bulletin of the Astronomical Institutes of the Netherlands **6**, 249 (1932).

[3] F. Zwicky, General Relativity and Gravitation **41**, 207 (2009).

[4] S. van den Bergh, Publ. Astron. Soc. Pac. **111**, 657 (1999), arXiv:astro-ph/9904251 [astro-ph] .

[5] S. Smith, Astrophys. J. **83**, 23 (1936).

[6] H. W. Babcock, Lick Observatory Bulletin **498**, 41 (1939).

[7] V. C. Rubin and J. Ford, W. Kent, Astrophys. J. **159**, 379 (1970).

[8] R. Massey, T. Kitching, and J. Richard, Reports on Progress in Physics **73**, 086901 (2010).

[9] A. G. Bergmann, V. Petrosian, and R. Lynds, Astrophys. J. **350**, 23 (1990).

[10] S. Faber and J. Gallagher, Annual Review of Astronomy and Astrophysics **17**, 135 (1979).

[11] D. Clowe, M. Bradač, A. H. Gonzalez, M. Markevitch, S. W. Randall, C. Jones, and D. Zaritsky, The Astrophysical Journal **648**, L109 (2006).

[12] M. Bradač, D. Clowe, A. H. Gonzalez, P. Marshall, W. Forman, C. Jones, M. Markevitch, S. Randall, T. Schrabback, and D. Zaritsky, Astrophys. J. **652**, 937 (2006), arXiv:astro-ph/0608408 [astro-ph] .

[13] G. Efstathiou, W. Sutherland, and S. Maddox, Nature **348**, 705 (1990).

[14] A. Arbey and F. Mahmoudi, Progress in Particle and Nuclear Physics **119**, 103865 (2021).

[15] G. Bertone, D. Hooper, and J. Silk, Physics Reports **405**, 279 (2005).

[16] J. L. Feng, Annual Review of Astronomy and Astrophysics **48**, 495 (2010).

[17] L. Perivolaropoulos and F. Skara, New Astronomy Reviews **95**, 101659 (2022).

[18] E. Hubble, Proceedings of the national academy of sciences **15**, 168 (1929).

[19] S. Dodelson, *Modern cosmology* (Academic Press, San Diego, CA, 2003).

[20] M. Trodden and S. M. Carroll, "Tasi lectures: Introduction to cosmology," (2004), arXiv:astro-ph/0401547 [astro-ph] .

[21] A. G. Riess, A. V. Filippenko, P. Challis, A. Clocchiatti, A. Diercks, P. M. Garnavich, R. L. Gilliland, C. J. Hogan, S. Jha, R. P. Kirshner, B. Leibundgut, M. M. Phillips, D. Reiss, B. P. Schmidt, R. A. Schommer, R. C. Smith, J. Spyromilio, C. Stubbs, N. B. Suntzeff, and J. Tonry, The Astronomical Journal **116**, 1009 (1998).

[22] S. Perlmutter, S. Gabi, G. Goldhaber, A. Goobar, D. E. Groom, I. M. Hook, A. G. Kim, M. Y. Kim, J. C. Lee, R. Pain, C. R. Pennypacker, I. A. Small, R. S. Ellis, R. G. McMahon, B. J. Boyle, P. S. Bunclark, D. Carter, M. J. Irwin, K. Glazebrook, H. J. M. Newberg, A. V. Filippenko, T. Matheson, M. Dopita, and W. J. C. and, The Astrophysical Journal **483**, 565 (1997).

[23] A. D. Chernin, Physics-Uspekhi **51**, 253 (2008).

[24] B. Ryden, *Introduction to cosmology* (Cambridge University Press, 1970).

[25] C. L. C. et al., "Snowmass2021 cosmic frontier: Cosmic microwave background measurements white paper," (2022), arXiv:2203.07638 [astro-ph.CO] .

[26] R. P. Feynman, R. B. Leighton, and M. Sands, "The Feynman lectures on physics; New millennium ed." (Basic Books, New York, NY, 2010) Chap. 45, originally published 1963-1965.

[27] E. W. Kolb and M. S. Turner, *The Early Universe*, Vol. 69 (CRC Press, 1990).

[28] L. Husdal, Galaxies **4**, 78 (2016).

[29] E. G. D. Cohen and W. Thirring, eds., *The Boltzmann Equation* (Springer Vienna, 2012).

[30] H. Lee, *Fundamentals Of Theoretical Plasma Physics: Mathematical Description Of Plasma Waves* (World Scientific Publishing Company, 2019).

[31] A. P. Lessa, "Boltzmann code docs," `https://github.com/andlessa/BoltzmannEqs` (2017).

[32] P. Gondolo and G. Gelmini, Nuclear Physics B **360**, 145 (1991).

[33] K.-C. Yang, Journal of High Energy Physics **2022** (2022), 10.1007/jhep11(2022)083.

[34] S. Hamdan and J. Unwin, Modern Physics Letters A **33**, 1850181 (2018).

[35] X. Chu, Y. Cui, J. Pradler, and M. Shamma, Journal of High Energy Physics **2022** (2022), 10.1007/jhep03(2022)031.

[36] D. Berger, S. Ipek, T. M. Tait, and M. Waterbury, Journal of High Energy Physics **2020** (2020), 10.1007/jhep07(2020)192.

[37] J. N. Howard, S. Ipek, T. M. P. Tait, and J. Turner, Journal of High Energy Physics **2022** (2022), 10.1007/jhep02(2022)047.

[38] Y. Du, F. Huang, H.-L. Li, Y.-Z. Li, and J.-H. Yu, Journal of Cosmology and Astroparticle Physics **2022**, 012 (2022).

[39] G. Arcadi, M. Dutra, P. Ghosh, M. Lindner, Y. Mambrini, M. Pierre, S. Profumo, and F. S. Queiroz, The European Physical Journal C **78** (2018), 10.1140/epjc/s10052-018-5662-y.

[40] M. Garny, J. Heisig, M. Hufnagel, B. Lülf, and S. Vogl, "Conversion-driven freeze-out: Dark matter genesis beyond the wimp paradigm," (2019), arXiv:1904.00238 [hep-ph] .

[41] M. Schumann, Journal of Physics G: Nuclear and Particle Physics **46**, 103003 (2019).

[42] K. Griest and D. Seckel, Phys. Rev. D **43**, 3191 (1991).

[43] N. F. Bell, Y. Cai, and A. D. Medina, Physical Review D **89** (2014), 10.1103/physrevd.89.115001.

[44] V. V. Khoze, A. D. Plascencia, and K. Sakurai, Journal of High Energy Physics **2017** (2017), 10.1007/jhep06(2017)041.

[45] R. T. D'Agnolo, C. Mondino, J. T. Ruderman, and P.-J. Wang, "Exponentially light dark matter from coannihilation," (2018), arXiv:1803.02901 [hep-ph] .

[46] S. Biondini and M. Laine, Journal of High Energy Physics **2018** (2018), 10.1007/jhep04(2018)072.

[47] W.-Y. Keung, I. Low, and Y. Zhang, Physical Review D **96** (2017), 10.1103/physrevd.96.015008.

[48] S. Mizuta and M. Yamaguchi, Physics Letters B **298**, 120 (1993).

[49] J. Ellis, F. Luo, and K. A. Olive, Journal of High Energy Physics **2015** (2015), 10.1007/jhep09(2015)127.

[50] R. T. D'Agnolo, D. Pappadopulo, and J. T. Ruderman, Physical Review Letters **119** (2017), 10.1103/physrevlett.119.061102.

[51] J. Heeck, J. Heisig, and A. Thapa, Physical Review D **107** (2023), 10.1103/physrevd.107.015028.

[52] M. Garny and J. Heisig, Physical Review D **105** (2022), 10.1103/physrevd.105.055004.

[53] F. Brümmer, Journal of High Energy Physics **2020** (2020), 10.1007/jhep01(2020)113.

[54] M. Garny, J. Heisig, B. Lülf, and S. Vogl, Physical Review D **96** (2017), 10.1103/physrevd.96.103521.

[55] N. Bernal, M. Heikinheimo, T. Tenkanen, K. Tuominen, and V. Vaskonen, International Journal of Modern Physics A **32**, 1730023 (2017).

[56] K. S. Babu, S. Chakdar, N. Das, D. K. Ghosh, and P. Ghosh, Journal of High Energy Physics **2023** (2023), 10.1007/jhep07(2023)143.

[57] C. E. Yaguna and Óscar Zapata, "A minimal model of fermion fimp dark matter," (2023), arXiv:2308.05249 [hep-ph] .

[58] L. J. Hall, K. Jedamzik, J. March-Russell, and S. M. West, Journal of High Energy Physics **2010** (2010), 10.1007/jhep03(2010)080.

[59] L. Lopez-Honorez, Q. Decant, S. Junius, and M. H. G. Tytgat, "Dark matter from wimp to fimp over three regimes: Cosmology versus colliders," (2022), arXiv:2212.12377 [hep-ph] .

[60] S. Enomoto, Y.-H. Su, M.-Z. Zheng, and H.-H. Zhang, (2023), arXiv:2301.11819 [hep-ph] .

[61] F. Hahn-Woernle, M. Plümacher, and Y. Wong, Journal of Cosmology and Astroparticle Physics **2009**, 028 (2009).

[62] K. Garrett and G. Duda, Advances in Astronomy **2011**, 1 (2011).

[63] J. L. Feng, Annual Review of Astronomy and Astrophysics **48**, 495 (2010), https://doi.org/10.1146/annurev-astro-082708-101659 .